Elastic and anelastic relaxations associated with the incommensurate structure of $Pr_{0.48}Ca_{0.52}MnO_3$

Michael A. Carpenter, Christopher J. Howard, and Ruth E. A. McKnight
Department of Earth Sciences, University of Cambridge, Downing Street, Cambridge CB2 3EQ, United Kingdom

Albert Migliori, Jon B. Betts, and Victor R. Fanelli
National High Magnetic Field Laboratory, Los Alamos National Laboratory, Los Alamos, New Mexico 87545, USA
(Received 29 June 2010; published 27 October 2010)

The elastic and anelastic properties of a polycrystalline sample of $Pr_{0.48}Ca_{0.52}MnO_3$ have been investigated by resonant ultrasound spectroscopy, as a function of temperature (10–1130 K) and magnetic field strength (0–15 T). Marked softening of the shear modulus as the $Pnma \leftrightarrow$ incommensurate phase transition at ~235 K in zero field is approached from either side is consistent with pseudoproper ferroelastic character, driven by an order parameter with Γ_3^+ symmetry associated with Jahn-Teller ordering. This is accompanied by an increase in attenuation just below the transition point. The attenuation remains relatively high down to ~80 K, where there is a distinct Debye peak. It is attributed to coupling of shear strain with the Γ_3^+ order parameter which, in turn, controls the repeat distance of the incommensurate structure. Kinetic data extracted from the Debye peak suggest that the rate-controlling process could be related to migration of polarons. Elastic softening and stiffening as a function of magnetic field at constant temperatures between 177 and ~225 K closely resembles the behavior as a function of temperature at 0, 5, and 10 T and is consistent with thermodynamically continuous behavior for the phase transition in both cases. This overall pattern can be rationalized in terms of linear/quadratic coupling between the Γ_3^+ order parameter and an order parameter with Σ_1 or Σ_2 symmetry. It is also consistent with a dominant role for spontaneous strains in determining the strength of coupling, evolution of the incommensurate microstructure, and equilibrium evolution of the Jahn-Teller ordered structure through multicomponent order-parameter space.

DOI: 10.1103/PhysRevB.82.134123 PACS number(s): 64.60.Ej, 62.40.+i, 62.20.de, 71.30.+h

I. INTRODUCTION

Phase transitions are by definition collective phenomena. Some local instability in the atomic or electronic configuration of a structure develops correlations over a significant length scale, macroscopic symmetry is broken, and a new long-range order is established. The most overt and predictable evidence for this is typically the development of both symmetry-breaking and nonsymmetry-breaking spontaneous strains (e.g., Ref. 1). An original atomic-scale interaction becomes a strain field, which then plays a fundamental role in determining thermodynamic behavior, microstructure, and physical properties. Such general truisms are as relevant for combined electronic and structural phase transitions in manganite perovskites, as for any other transitions. Changes in electronic configuration which give rise to charge order, magnetization, and metal/insulator behavior are associated with characteristic local and macroscopic strain effects, providing a consistent theme through many treatments of their overall phenomenological diversity (e.g., Refs. 2–13). It follows that the overall structural evolution of these materials and relationships between their structure and physical properties will depend on the symmetry and strength of strain/order-parameter coupling.

A further encompassing aspect of the transition behavior of manganites has been their response to applied magnetic fields. Within solid solutions such as $La_{1-x}Ca_xMnO_3$ and $Pr_{1-x}Ca_xMnO_3$ (PCMO), there is competition between a ferromagnetic structure and an incommensurate structure or its commensurate equivalent (e.g., Refs. 4, 8, and 14–18). For selected ranges of compositions and at low temperatures, conversion from a charge ordered insulator state to a ferromagnetic metal can be driven by increasing magnetic field strength (e.g., Refs. 19–22). The metal/insulator transition is accompanied by significant elastic strains, measured as magnetostriction (e.g., Refs. 23–26), and by marked changes in elastic properties (e.g., Refs. 27–31). It follows, again, that the structural evolution must be influenced by, or even governed by strain/order-parameter coupling in spite of the electronic nature of the changes in magnetization and electrical conductivity.

Strain/order-parameter coupling dominates the properties and behavior of ferroelastic materials and it has recently been shown that the $Pnma \leftrightarrow$ incommensurate (IC) phase transition in $Pr_{0.48}Ca_{0.52}MnO_3$ (Pr48) can be analyzed from the same point of view.[32] Following a complete group theoretical treatment,[33] structural evolution of the IC phase was found to depend on order parameters relating to two separate octahedral tilting mechanisms [belonging to irreducible representations (irreps) M_3^+ and R_4^+], two distinct cooperative Jahn-Teller ordering schemes (irrep's M_2^+ and Γ_3^+) and to the symmetry-breaking order parameter itself (irrep Σ_1 or Σ_2). Individual symmetry-adapted strains extracted from high-resolution lattice parameter data revealed that the evolution of these order parameters conforms with Landau theory and that the transition can be described as being close to tricritical in character with respect to the Σ order parameter. The repeat distance of the IC structure has also turned out to scale simply with the Γ_3^+ order parameter.

Strain is an equilibrium property which depends only on the first derivative of free energy. A much more stringent test of any order-parameter model for a phase transition is provided by comparisons of observed and predicted variations in elastic constants. These are second derivatives and define

the curvature of the free-energy potential around the equilibrium point rather than simply the locus of equilibrium point itself. Patterns of elastic constants vary widely between proper ferroelastic, pseudoproper ferroelastic, improper ferroelastic, and coelastic transitions, as well as between first order, tricritical, and second-order transitions (e.g., Refs. 34–38). In this context, the $Pnma \leftrightarrow$ IC transition and the transition to the related commensurate phase in $Pr_{1-x}Ca_xMnO_3$ are coelastic and should have an entirely predictable pattern of elastic softening or stiffening. What is actually observed, however, is substantial softening of shear elastic constants as the transition is approached from either side with a pattern that is typical of pseudoproper ferroelastic behavior.[29,39–52] This further emphasizes the importance of the (zone center) Γ_3^+ order parameter in controlling the structural evolution, even though it is not symmetry breaking. Having established the nature of strain coupling with the different macroscopic order parameters in detail,[32] the purpose of the present paper is to revisit the elastic behavior of these materials, with and without a strong magnetic field, and to determine whether the overall structural evolution is indeed governed by strain/order-parameter coupling.

Resonant ultrasound spectroscopy (RUS) has been used here to characterize elastic anomalies that accompany the $Pnma \leftrightarrow$ IC transition in Pr48, both as a function of temperature and as a function of magnetic field strength up to 15 T. This specific material was chosen because it is far from any known two phase field, the ordered structure remains incommensurate at all temperatures,[53] there are data available for the heat capacity[54] and magnetization,[53] its microstructure has been characterized by transmission electron microscopy,[53,55] and the antiferromagnetic transition ($T_N \approx 180$ K in $Pr_{0.5}Ca_{0.5}MnO_3$)[21,26,56] occurs significantly below the structural transition temperature ($T_c \approx 235$ K). Interpretation of the elastic properties is also informed by the detailed understanding of strain/order-parameter evolution deduced from high-resolution lattice parameter data collected from the same sample.[32] The starting point is a simple Landau model which separates the roles of cooperative Jahn-Teller order and incommensurate displacements. In addition to providing data for the elastic properties, RUS gives information about dynamic aspects of the IC structure through acoustic dissipation effects expressed in terms of the mechanical quality factor, Q.

II. LANDAU THEORY FOR PSEUDOPROPER FERROELASTIC CHARACTER

Irrespective of whether the commensurate ordered phase of half-doped manganites such as $Pr_{0.5}Ca_{0.5}MnO_3$ (Pr50) has $Pnm2_1$ or $P2_1/m$ symmetry, the phase transition from the parent $Pnma$ phase to the ordered phase is associated with a zone boundary point. This is the X point of the Brillouin zone for $Pnma$.[15,32] The Landau expansion for excess free energy, including lowest order coupling to strains, e_i, would be

$$G = \frac{1}{2}a\Theta_s\left[\coth\left(\frac{\Theta_s}{T}\right) - \coth\left(\frac{\Theta_s}{T_c}\right)\right](q_1^2+q_2^2) + \frac{1}{4}b(q_1^2+q_2^2)^2 + \frac{1}{4}b'(q_1^4+q_2^4) + d\left(q_1\frac{\partial q_2}{\partial x} - q_2\frac{\partial q_1}{\partial x}\right) + \frac{e}{2}[(\nabla q_1)^2 + (\nabla q_2)^2] + (\lambda_1 e_1 + \lambda_2 e_2 + \lambda_3 e_3)(q_1^2+q_2^2) + \lambda_4 e_4^2(q_1^2+q_2^2) + \lambda_5 e_5(q_1^2-q_2^2) + \lambda_6 e_6^2(q_1^2+q_2^2) + \frac{1}{2}\sum_{i,k=1-6} C_{ik}^o e_i e_k, \quad (1)$$

where q_i are order-parameter components, Θ_s is the order-parameter saturation temperature, λ_i are coupling coefficients, x is the direction of the crystallographic x axis, and C_{ik}^o are elastic constants of the $Pnma$ structure. The $P2_1/m$ product phase would have $q_1 \neq 0$, $q_2 = 0$, the $Pnm2_1$ phase would have $q_1 = q_2 \neq 0$, and $q_1 \neq q_2 \neq 0$ would give Pm. A $Pnma \leftrightarrow Pnm2_1$ transition would be coelastic and a $Pnma \leftrightarrow P2_1/m$ transition would be improper ferroelastic. The strain/order-parameter coupling terms are all of the form λeq^2 or λe^2q^2 and would not give rise to elastic softening as the transition point is approached from above. The transitions should be marked by discontinuities of the elastic constants arising from the λeq^2 coupling and continuous variations in elastic constants arising from λe^2q^2 (see, for example, Carpenter and Salje[38]). The latter will generally be small. The transition to a commensurate phase is expected to be first order due to the existence of the Lifshitz invariants.[57] Strain coupling terms for an order parameter representing the amplitude of the IC phase would have the same form but the transition can be second order because the weak Lifshitz condition for second-order character is no longer violated.[58]

The phase transition near ~230 K in $Pr_{1-x}Ca_xMnO_3$ with $x=0.35$ or 0.4 is expected to be to the commensurate structure[59,60] while the product phase is incommensurate at $x=0.5$.[60–64] In both cases, the transition is marked by elastic softening of average cubic values of $\frac{1}{2}(C_{11}-C_{12})$ in single crystals as $T \rightarrow T_c$ from above.[39,40] On the basis of neutron diffraction and transmission electron microscopy observations on selected samples[53,59,61,65] the phase transition in crystals with $0.5 < x < 0.85$ (Pr50-Pr15) is expected to be to the incommensurate structure. Measurements of longitudinal ultrasonic velocities in polycrystalline samples within this range also reveal elastic softening ahead of the transition.[41,42] In each case, the pattern of softening is typical of a pseudoproper ferroelastic transition and has the form (not including an order-parameter saturation term)

$$(C_{11}-C_{12}) = (C_{11}^o - C_{12}^o)\left(\frac{T-T_c^*}{T-T_c}\right), \quad (2)$$

where $(C_{11}^o - C_{12}^o)$ refers to the parent structure and T_c^* is the critical temperature renormalized by bilinear coupling of driving order parameter, Q, with the symmetry-breaking strain, e_{sb}, i.e., $\lambda e_{sb}Q$.[38,66,67] This form of expression has been used in treatments of the manganite charge-ordering transition.[39,40,42,50–52,68] The physical origin of the zone center relaxation was attributed to the quadrupolar moment of Mn^{3+}, with T_c^*, T_c representing characteristic temperatures which are understood in terms of a susceptibility and specific

coupling effects among phonons, Jahn-Teller ions and strain.[68]

Equation (2) does not follow from Eq. (1) and a generalized Landau treatment of the elastic properties of Pr48 requires inclusion of a zone center order parameter with some bilinear strain/order-parameter coupling. The relevant symmetry-breaking strain and order parameter belong to irrep Γ_3^+ of the $Pm\bar{3}m$ reference state (E_g symmetry in Hazama *et al.*[68]). From Table II of Carpenter *et al.*[32] it is apparent, however, that this symmetry is already broken in space group *Pnma*, implying that a Γ_3^+ order parameter would not normally be the driving order parameter for a further transition. Jahn-Teller transitions appear to provide an exception to this general rule in that, because of the highly localized origin of an electronic instability, it appears to be possible to have a *Pnma* structure with macroscopic Jahn-Teller order parameters which are strictly zero. For example, there is a first-order $Pnma \leftrightarrow Pnma$ transition driven by the M_2^+ order parameter at ~750 K in $LaMnO_3$.[69–78] Doping of $LaMnO_3$ with Ba leads to a change from first-order to second-order character for the same transition.[78]

The Γ_3^+ order parameter relates to an ordered arrangement of uniaxially deformed octahedra with their unique axes all aligned parallel to [010] of the *Pnma* cell.[32,78–80] By itself it would cause a first-order transition from the parent cubic structure, $Pm\bar{3}m \leftrightarrow P4/mmm$, with a single nonzero order-parameter component, q_{tx}, and a tetragonal strain, e_{tx}, where

$$e_{tx} = \frac{1}{\sqrt{3}}(2e_1 - e_2 - e_3). \tag{3}$$

The linear strains e_1, e_2, and e_3 are specified with respect to cubic reference axes in the orientation given by Carpenter *et al.*[32] As shown schematically in Fig. 1, $(C_{11}-C_{12})$ would soften according to Eq. (2) as $T \rightarrow T_c^*$ from above, due to bilinear coupling $\lambda e_{tx} q_{tx}$, followed by recovery below a first-order transition at $T_{tr\,\Gamma}$. In reality, the transition occurs before $(C_{11}-C_{12})$ reaches zero and the total strain evolution and elastic softening at the $Pnma \leftrightarrow$ IC transition in Pr48 must depend on the combined effects of zone center and zone boundary order parameters. Thus it is necessary to develop a Landau expansion which includes both the X point and Γ_3^+ order parameters in order to understand the evolution of spontaneous strains and patterns of elastic softening/stiffening.

The X-point irrep of space group *Pnma* becomes Σ_1 or Σ_2 with respect to a $Pm\bar{3}m$ parent structure.[33] Each of the Σ_1 and Σ_2 order parameters contains two nonzero components for the structures of interest and the Landau free-energy expansion again contains gradient terms. The macroscopic strain behavior does not depend on whether the product structure is commensurate or incommensurate so, for convenience, the gradient terms are dropped here. On the basis of symmetry alone, it is not possible to distinguish between the influence of Σ_1 and Σ_2 in specific structural terms,[32] and the following development applies to both. In addition, the commensurate structure is taken as having $Pnm2_1$ symmetry (following Refs. 32 and 81–84) with $q_{1\Sigma}=q_{2\Sigma}$ for the Σ order parameter. These simplifications lead to a single Landau expansion, as expressed with respect to a cubic reference state but still referring to a phase transition in the *Pnma* structure, with the form

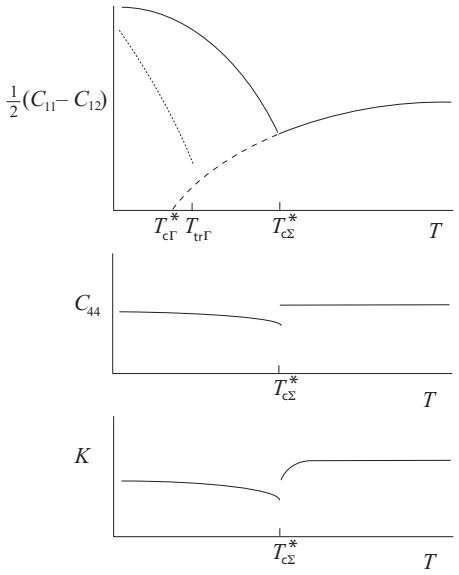

FIG. 1. Schematic variation in average cubic elastic constants through the structural phase transition of PCMO. A pure Jahn-Teller transition driven by the Γ_3^+ order parameter would be expected to show softening of $\frac{1}{2}(C_{11}-C_{12})$ down to a first-order transition at $T_{tr\,\Gamma}$. This degree of softening is not achieved because of the intervention of the Σ order parameter at $T_{c\Sigma}^*$. The broken line represents the extrapolation of the high-temperature softening and the dotted line represents recovery in the pure Jahn-Teller structure. C_{44} and K would be expected to show small discontinuities at T_c because of weak coupling of the order parameters with the e_4 and volume strains.

$$\begin{aligned} G = {} & \frac{1}{2}a_\Gamma \Theta_{s\Gamma}\left[\coth\left(\frac{\Theta_{s\Gamma}}{T}\right) - \coth\left(\frac{\Theta_{s\Gamma}}{T_{c\Gamma}}\right)\right]q_{tx}^2 - \frac{1}{3}u_\Gamma q_{tx}^3 \\ & + \frac{1}{4}b_\Gamma q_{tx}^4 + \lambda_{1\Gamma} e_a q_{tx}^2 + \lambda_{2\Gamma} e_{tx} q_{tx} + \lambda_{3\Gamma} e_{ox}^2 q_{tx}^2 + \lambda_{4\Gamma}(-2e_4^2 \\ & + e_6^2 + e_5^2)q_{tx} + \frac{1}{2}a_\Sigma \Theta_{s\Sigma}\left[\coth\left(\frac{\Theta_{s\Sigma}}{T}\right) - \coth\left(\frac{\Theta_{s\Sigma}}{T_{c\Sigma}}\right)\right]q_\Sigma^2 \\ & + \frac{1}{4}b_\Sigma q_\Sigma^4 + \lambda_{1\Sigma} e_a q_\Sigma^2 + \lambda_{2\Sigma} e_{tx} q_\Sigma^2 + \lambda_{3\Sigma} e_{ox}^2 q_\Sigma^2 + \lambda_{4\Sigma} e_4 q_\Sigma^2 \\ & + \lambda_{5\Sigma}(e_5^2 + e_6^2)q_\Sigma^2 + \lambda_{6\Sigma} e_5 e_6 q_\Sigma^2 + \lambda_{\Sigma\Gamma} q_{tx} q_\Sigma^2 + \frac{1}{4}(C_{11}^o - C_{12}^o) \\ & \times (e_{tx}^2 + e_{ox}^2) + \frac{1}{6}(C_{11}^o + 2C_{12}^o)e_a^2 + \frac{1}{2}C_{44}^o(e_4^2 + e_5^2 + e_6^2), \end{aligned} \tag{4}$$

where $e_{ox}=e_2-e_3$. The two order parameters are shown as having different critical temperatures, $T_{c\Gamma}$ and $T_{c\Sigma}$, different order-parameter saturation temperatures, and separate coupling with symmetry-adapted strains. The lowest order direct coupling term is linear/quadratic, $\lambda_{\Sigma\Gamma} q_{tx} q_\Sigma^2$. Applying the normal equilibrium condition, $\partial G/\partial e=0$, to obtain strain/order-parameter relationships and substituting back into Eq. (4) gives (with $e_5=e_6=e_{ox}=0$ and assuming $C_{44}^o \gg 4\lambda_{4\Gamma} q_{tx}$)

$$G = \frac{1}{2}a_\Gamma \Theta_{s\Gamma}\left[\coth\left(\frac{\Theta_{s\Gamma}}{T}\right) - \coth\left(\frac{\Theta_{s\Gamma}}{T^*_{c\Gamma}}\right)\right]q_{tx}^2 - \frac{1}{3}u_\Gamma q_{tx}^3 + \frac{1}{4}b^*_\Gamma q_{tx}^4 + \frac{1}{2}a_\Sigma \Theta_{s\Sigma}\left[\coth\left(\frac{\Theta_{s\Sigma}}{T}\right) - \coth\left(\frac{\Theta_{s\Sigma}}{T_{c\Sigma}}\right)\right]q_\Sigma^2 + \frac{1}{4}b^*_\Sigma q_\Sigma^4 + \lambda^*_{\Sigma\Gamma} q_{tx} q_\Sigma^2 + \lambda'^*_{\Gamma\Sigma} q_{tx}^2 q_\Sigma^2, \quad (5)$$

where

$$T^*_{c\Gamma} = T_{c\Gamma} + \frac{\lambda_{2\Gamma}^2}{a\frac{1}{2}(C^o_{11} - C^o_{12})}, \quad (6)$$

$$b^*_\Gamma = b_\Gamma - \frac{2\lambda_{1\Gamma}^2}{\frac{1}{3}(C^o_{11} + 2C^o_{12})}, \quad (7)$$

$$b^*_\Sigma = b_\Sigma - \frac{2\lambda_{1\Sigma}^2}{\frac{1}{3}(C^o_{11} + 2C^o_{12})} - \frac{2\lambda_{2\Sigma}^2}{\frac{1}{2}(C^o_{11} - 2C^o_{12})} - \frac{2\lambda_{4\Sigma}^2}{C^o_{44}}, \quad (8)$$

$$\lambda^*_{\Gamma\Sigma} = \lambda_{\Gamma\Sigma} - \frac{\lambda_{2\Gamma}\lambda_{2\Sigma}}{\frac{1}{2}(C^o_{11} - C^o_{12})}, \quad (9)$$

$$\lambda'^*_{\Gamma\Sigma} = -\frac{\lambda_{1\Sigma}\lambda_{1\Gamma}}{\frac{1}{3}(C^o_{11} + 2C^o_{12})}. \quad (10)$$

The equilibrium evolution with temperature for both order parameters is determined by the conditions

$$\frac{\partial G}{\partial q_{tx}} = 0 = a_\Gamma \Theta_{s\Gamma}\left[\coth\left(\frac{\Theta_{s\Gamma}}{T}\right) - \coth\left(\frac{\Theta_{s\Gamma}}{T^*_{c\Gamma}}\right)\right]q_{tx} - u_\Gamma q_{tx}^2 + b^*_\Gamma q_{tx}^3 + \lambda^*_{\Sigma\Gamma} q_\Sigma^2 + 2\lambda'^*_{\Gamma\Sigma} q_{tx} q_\Sigma^2, \quad (11)$$

$$\frac{\partial G}{\partial q_\Sigma} = 0 = a_\Sigma \Theta_{s\Sigma}\left[\coth\left(\frac{\Theta_{s\Sigma}}{T}\right) - \coth\left(\frac{\Theta_{s\Sigma}}{T_{c\Sigma}}\right)\right]q_\Sigma + b^*_\Sigma q_\Sigma^3 + 2\lambda^*_{\Sigma\Gamma} q_{tx} q_\Sigma + 2\lambda'^*_{\Gamma\Sigma} q_{tx}^2 q_\Sigma. \quad (12)$$

A quantitative description of the structural evolution would be obtained by solving Eqs. (11) and (12) for known values of the various coefficients, as in the case of bilinear coupling in the mineral albite[85,86] or for biquadratic coupling more generally.[87] Here the order-parameter coupling is linear/quadratic and, even if the direct coupling coefficient, $\lambda_{\Gamma\Sigma}$, is negligibly small, strong coupling is likely because both order parameters are coupled to the common tetragonal strain, e_{tx}, which is large [up to ~3% (Ref. 32)]. Biquadratic coupling is also assured due to coupling with the common volume strain, e_a, but is likely to be weak because $\lambda_{1\Gamma}$ and $\lambda_{1\Sigma}$ are small [$e_a < 0.2\%$ (Ref. 32)]. Linear/quadratic coupling has been investigated for the specific case of coupling between nonconvergent cation order and a displacive transition in the mineral pigeonite, where the principal influence of a fixed degree of order is to renormalize the displacive transition temperature.[88] It also occurs in $PrAlO_3$.[79] A more general treatment has not been attempted but the influence of q_{tx} will be to renormalize $T_{c\Sigma}$ to some higher value, $T^*_{c\Sigma}$, for favorable coupling while the effect of q_Σ^2 on q_{tx} will be equivalent to the influence of an externally applied field. This treatment differs from that of Hazama *et al.*[40] in having a second general order parameter to describe the IC phase rather than a specific order parameter related directly to charge ordering. It differs from the treatments of Zhong and Wang[15] or Milward *et al.*[8] in having the IC structure being stabilized by tetragonal Jahn-Teller distortions of the octahedra with all the unique axes aligned parallel to the crystallographic *y* axis of the *Pnma* structure, plus coupling of this with the Σ order parameter. Charge ordering is allowed but is not required.

According to Eq. (4), the *Pnma*↔IC transition has aspects of pseudoproper and improper ferroelastic character as a consequence of the different coupling of the individual order parameters with the spontaneous strains, with immediate consequences for the evolution of the elastic constants. Considering only average cubic elastic constants, $(C_{11} - C_{12})$ will soften according to Eq. (2) until the actual transition temperature, $T^*_{c\Sigma}$. The bulk modulus, $K = \frac{1}{3}(C_{11} + 2C_{12})$, would be also be expected to show some softening ahead of the transition according to

$$K - K_o = A(T - T^*_{c\Sigma})^\kappa, \quad (13)$$

where A and κ are material constants. The value of κ is sensitive both to the degree of anisotropy of dispersion curves about the reciprocal lattice vector of the critical point and the extent of any softening along each branch (see Ref. 38, and references therein). To first order, C_{44} would not be expected to show any softening but fluctuations are likely to cause some small changes in the close vicinity of the transition point. Softening due to fluctuations just ahead of a transition point is well illustrated by the examples of $LaAlO_3$,[89] $SrTiO_3$, and $KMnF_3$ (see, for example, summaries of data in Ref. 38).

Behavior of the elastic constants below the transition temperature will follow patterns set out in Fig. 1 of Carpenter and Salje[38] and are illustrated schematically in Fig. 1 of the present paper. In the absence of coupling between q_{tx} and q_Σ, $(C_{11} - C_{12})$ would have a discontinuity at some transition point, $T_{tr\,\Gamma}$, with subsequent stiffening. The *Pnma*↔IC transition occurs at $T^*_{c\Sigma}$, however, and then $(C_{11} - C_{12})$ will stiffen due to the bilinear coupling $\lambda_{2\Gamma} e_{tx} q_{tx}$. K will soften discontinuously due to $\lambda_{1\Gamma} e_a q_{tx}^2$ and $\lambda_{1\Sigma} e_a q_\Sigma^2$. C_{44} will show a small, continuous change (stiffening or softening, depending on the sign of the strain coupling coefficients) due to $\lambda_{4\Gamma}(-2e_4^2 + e_6^2 + e_5^2)q_{tx}$ and $[\lambda_{5\Sigma}(e_5^2 + e_6^2) + \lambda_{6\Sigma} e_5 e_6]q_\Sigma^2$, with a small discontinuous softening due to $\lambda_{4\Sigma} e_4 q_\Sigma^2$. For small e_4 strains, the variation in shear modulus, G, should effectively reflect the variation in $(C_{11} - C_{12})$.

According to Krupicka *et al.*[56] the Néel temperature of Pr50 and the Curie temperature, estimated from the paramagnetic susceptibility, are both below T_c. Magnetization is not a requirement for stability, therefore. On the contrary, the structural phase transition is suppressed by application of a

magnetic field in a manner that can be explained in terms of unfavorable coupling between a ferromagnetic order parameter, M, and structural order parameters (e.g., Refs. 8 and 15). In the present context, the important question is how M couples with q_{tx} and q_{Σ}. Bilinear coupling of M with a strain only occurs in piezomagnetic materials and is restricted to antiferromagnetically ordered phases with specific magnetic symmetry.[90] Normal magnetostriction involves linear/quadratic coupling, $\lambda e M^2$. The volume strain e_a can couple separately with M^2 and q_{Σ}^2, leading to biquadratic coupling between them, $\lambda_{q\Sigma,M} q_{\Sigma}^2 M^2$. Linear/quadratic coupling of the Jahn-Teller and structural order parameters, $\lambda_{qtx,\Sigma} q_{tx} q_{\Sigma}^2$, is permitted and it follows that $\lambda_{qtx,M} q_{tx} M^2$, which is the direct coupling equivalent of indirect coupling through a common strain as $\lambda e_{tx} q_{tx}$ and $\lambda e_{tx} M^2$, must also be allowed. Both $\lambda_{q\Sigma,M} q_{\Sigma}^2 M^2$ and $\lambda_{qtx,M} q_{tx} M^2$ can be energetically unfavorable but, because q_{tx} and M both arise from electronic effects, $\lambda_{qtx,M} q_{tx} M^2$ is likely to be the more physically significant. This would also cause suppression of the pseudoproper acoustic softening above the transition point with increasing magnetic field strength, as is indeed observed (see below).

The influence of magnetic field, H, should be understandable through the addition of the following terms to Eq. (5) (after Ref. 91)

$$-HM + \frac{1}{2\chi(T)} M^2 + \frac{1}{4} b_M M^4 + \cdots + \lambda_{qtx,M} q_{tx} M^2,$$

where the temperature dependence of M, independently of coupling with q_{tx}, is expressed in terms of some susceptibility, $\chi(T)$. The conditions for equilibrium with respect to temperature and magnetic field strength are then given by $\frac{\partial G}{\partial q_{tx}} = 0$, $\frac{\partial G}{\partial M} = 0$, etc., in the usual way. Strong coupling between q_{tx} and q_{Σ}^2 will ensure suppression of the structural phase transition when coupling between q_{tx} and M is unfavorable. General solutions for this linear/quadratic coupling system in an applied field do not appear to have been developed as yet, but three solutions are expected: $q_{tx} \neq 0$ with $M=0$, $q_{tx}=0$ with $M \neq 0$ and a mixed state, $q_{tx} \neq 0$, $M \neq 0$. The transition from $q_{tx} \neq 0$, $M \neq 0$ to the structure with $q_{tx}=0$, $q_{\Sigma}=0$ might be discontinuous or continuous, as illustrated schematically in Fig. 2.

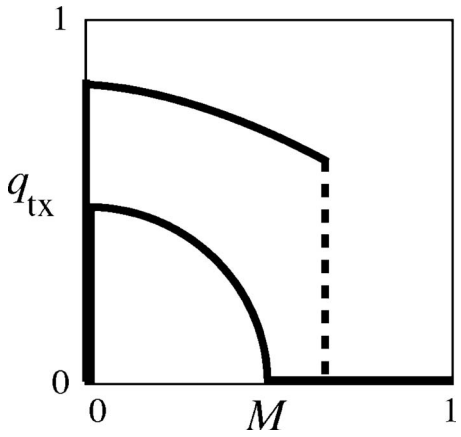

FIG. 2. Schematic order-parameter variations for intermediate members of the $Pr_{1-x}Ca_xMnO_3$ solid solution under the influence of magnetic field strength at low temperatures. With falling temperature below the structural phase transition temperature, $T_{c\Sigma}^*$, the Γ_3^+ order parameter (q_{tx}) increases from zero. Application of a magnetic field then causes an increase in the magnetic order parameter, M. At low temperatures and for commensurate ordered structures, the structure with $M \neq 0$, $q_{tx}=0$ develops at a first-order discontinuity (broken line) whereas for incommensurate structures the transition appears to be continuous (solid curve).

III. EXPERIMENTAL METHODS

The sample of $Pr_{0.48}Ca_{0.52}MnO_3$ was purchased from Pi-Kem Ltd., U.K. It had been produced by Praxair, U.S.A., using the Combustion Spray Pyrolysis process in which a mixture of nitrates was mixed with a carbohydrate solution that was subsequently dehydrated and combusted. The resultant powder was consolidated by cold isostatic pressing in a die press, and fired in air at ~1300 °C. Parallelepipeds were cut from two different fired pellets using a fine annular diamond saw lubricated with paraffin: PCMO1: $3.143 \times 2.864 \times 1.587$ mm^3, 0.0756 g, PCMO2: $3.215 \times 2.984 \times 2.872$ mm^3, 0.1457 g. Densities determined from these dimensions and masses are 5.292, 5.288 g cm^{-3}, which correspond to 92.2% of the theoretical density (5.736 g cm^{-3}), as calculated using room temperature lattice parameters from Carpenter *et al.*[32] and assuming full stoichiometry. The powder x-ray (Cu $K\alpha$) diffraction pattern obtained from a ground up offcut from a pellet contained peaks corresponding to perovskite with the *Pnma* structure. Apart from a possible weak peak at $2\theta \approx 28.6°$, there was no obvious evidence for the presence of other phases. The average grain size obtained by measuring 100 grains in scanning electron microscope images from two broken surfaces of another offcut was 1.4 μm; the smallest and largest grains observed had widths of ~0.6 and ~2.2 μm, respectively. The Ca:Mn ratio was checked by electron microprobe analysis of a polished sample (0.516:1) and the Pr:Mn ratio was checked by ICPMS of a sample dissolved in acid (0.479:1). Both these ratios are within experimental uncertainty of the expected composition.

RUS spectra were collected from both samples *in situ* at low and high temperatures in Cambridge. The He cryostat and DRS M^{3}ODULUS II electronics used for the low-temperature instrument have been described by McKnight *et al.*[92] The high-temperature instrument has been described by McKnight *et al.*,[93] including calibration of temperature against the transition point of quartz.[94] For low-temperature data collections, a parallelepiped was held lightly between the piezoelectric transducers across opposite corners or opposite faces. In the high-temperature instrument, the parallelepiped was supported lightly across its corners between alumina rods protruding into a horizontal furnace. Spectra were transferred to the software package IGOR PRO (Wavemetrics) for analysis. Peak frequencies were determined by inspection for calculation of bulk and shear moduli using the DRS software described by Migliori and Sarrao.[95] Selected peaks were also fit with an asymmetric Lorentzian function to determine peak frequency, f, and peak width at half height, Δf, and hence to determine values for the mechanical quality factor, Q, where $Q = f/\Delta f$.

RUS spectra were collected from sample PCMO2 in two different Oxford Instruments superconducting magnets at fields up to 15 T in Los Alamos. The parallelepiped was held across a pair of faces in a spring loaded RUS head at the end of a stick which was lowered into the magnet. Stress on the sample from spring loading was sufficient to hold the sample in place but small enough to not destroy the free boundary elastic condition. Temperature control was achieved by a helium-4 flow cryostat and an Oxford ITC 503 controller. A Stanford Research Systems DS345 function generator and SR844 lock-in amplifier were used to excite and detect the resonance frequencies.[95,96] The frequencies and widths at half height were obtained for selected peaks by fitting with inhouse software (available at http://www.magnet.fsu.edu/inhouseresearch/rus/index.html).

IV. RESULTS

A. Room temperature

Frequencies of the first 36 resonance peaks (20 000 data points collected between 100 and 1200 kHz) from PCMO2 were measured at room temperature and gave values of $K=117.6$ GPa and $G=43.9$ GPa, with an rms error of 0.13%. Correction for 7.8% porosity, using the expressions of Ledbetter *et al.*,[97] gave $K=149.5$ and $G=50.8$ GPa for a fully dense sample. These values compare with $K=135$ and $G=44$ GPa given by Seiro *et al.*[29] for a ceramic sample of Pr65 with 90% of theoretical density prepared by heating at 1300 °C for five days in oxygen. Single-crystal elastic constants have been reported as average cubic values for Pr50 by Hazama *et al.*,[39] giving Voigt/Reuss/Hill averages of $K=31.9$ GPa and $G=16.3$ GPa at room temperature. The reason for such a large discrepancy between the data for single crystal and ceramic samples is not clear. Ceramic samples of $La_{1-x}Ca_xMnO_3$ with ~10% porosity have $K\sim 50-65$ GPa and $G\sim 35$ GPa for $0<x<1$.[98]

B. Variable temperature, without magnetic field (Cambridge)

Figure 3 contains a stack of spectra obtained from PCMO1 between 10 K and room temperature (50 000 data points per spectrum). They were collected in a heating sequence with 5 or 2 K steps and an equilibration period of 15 min at each temperature. The phase transition near 235 K is clearly associated with a change in trend of the peak frequencies and widths. Values of G were then obtained for the entire temperature range by scaling (frequency)^2 for the peak near 670 kHz at room temperature, using the room temperature (293 K) value of $G=43.9$ GPa from peak fitting. Values of Q^{-1} were obtained from the same peak, which increased to ~850 kHz at 10 K. These are shown in Fig. 4, to which has been added $T_N=180$ K for antiferromagnetic ordering in Pr50 (Refs. 21, 26, 56, and 64) and $T^*_{c\Sigma}=237$ K for the structural phase transition in Pr48.[32] The shear modulus softens as $T\rightarrow T^*_{c\Sigma}$ but reaches a minimum value just below the expected transition temperature. A continuous stiffening trend is then followed with further decrease in temperature. Dissipation is low in the stability field of the *Pnma* phase above ~250 K, but Q^{-1} then increases, with the steepest slope occurring below the temperature at which G reaches its minimum value. Below $T^*_{c\Sigma}$, Q^{-1} remains near ~0.01, with some variation which is probably experimental scatter. There is a Debye-type peak in Q^{-1} at ~75 K which coincides with a small increase in G. At the lowest temperatures, Q^{-1} returns to the low values of the high-temperature phase. There are no

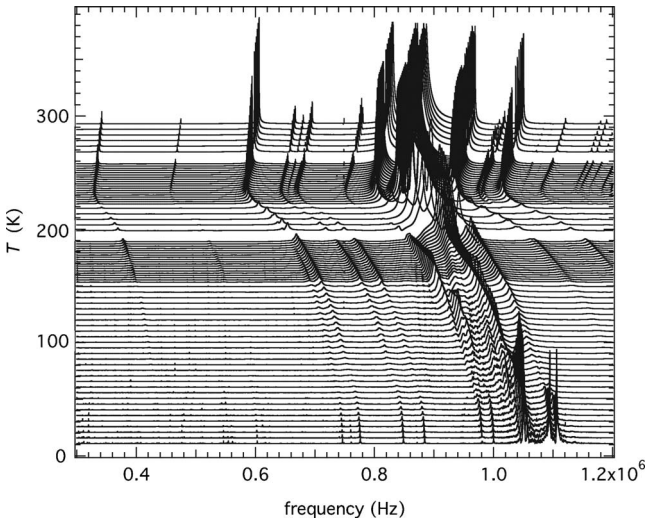

FIG. 3. Stack of RUS spectra obtained from sample PCMO1. The y axis is really amplitude but spectra have been displaced in proportion to the temperature at which they were collected and the axis is labeled as temperature. Weak peaks at low frequencies and low temperatures are noise. The structural phase transition is evident from a change in trend of frequency with temperature for all the resonance peaks at ~230 K. Significant peak broadening, due to attenuation, is also clearly associated with the transition. Further peak broadening is also evident between ~40 and ~90 K.

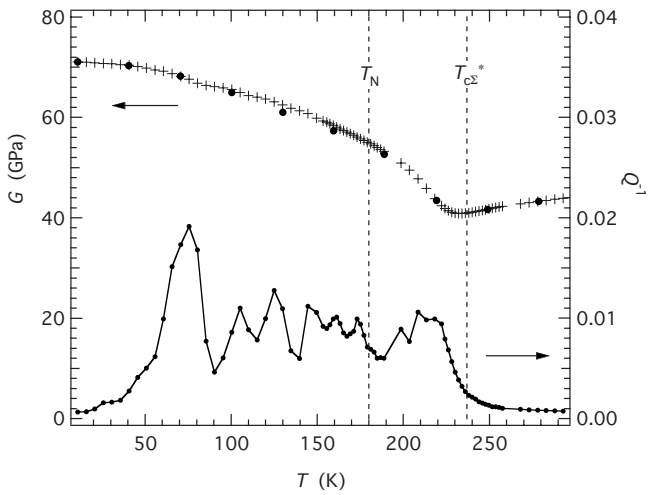

FIG. 4. Variation in the shear modulus, G, and inverse mechanical quality factor, Q^{-1}, extracted from fitting of the frequency and line width of the resonance peak in Fig. 2 which has $f=667$ kHz at room temperature. Filled circles represent G from spectra collected during cooling and crosses represent G obtained from spectra collected during heating. There is a small hysteresis between ~100 and ~200 K. Dots joined by lines are data for Q^{-1} obtained during heating; scatter in absolute values through the interval 90–210 K is probably due to noise in the baseline of the primary spectra.

obvious features near the expected antiferromagnetic transition point. Also shown in Fig. 4 are values of G at 30 K intervals from the cooling run, prior to the main data collection during heating. The equilibration time for data collection at each temperature was 20 min. These data reveal a small hysteresis, with the shear modulus being slightly lower during cooling than during heating between ~100 and ~200 K.

The Debye peak has been fit in a conventional manner to obtain an estimate of the activation energy, E_a, and the reciprocal of the attempt frequency, τ_o, for a thermally activated process conforming to

$$\tau = \tau_o \exp\left(\frac{E_a}{RT}\right), \tag{14}$$

where τ is the relaxation time at temperature T. The Debye peak itself is expected to depend on the angular frequency, $\omega(=2\pi f)$, of an applied stress according to

$$Q^{-1} = \Delta \frac{\omega\tau}{1+\omega^2\tau^2}. \tag{15}$$

In the case of a standard linear solid

$$\Delta = \frac{C_U - C_R}{C_R} \quad \text{for } (C_U - C_R \ll C_R), \tag{16}$$

where C_U is the relevant elastic modulus for the unrelaxed state and C_R the elastic modulus of the relaxed state.[99] The maximum value of Q^{-1}, Q_m^{-1}, occurs at temperature T_m, and is equal to $\Delta/2$. A single peak measured as a function of temperature at approximately constant frequency can be described by (from Refs. 100 and 101)

$$Q^{-1}(T) = Q_m^{-1}\left[\cosh\left\{\frac{E_a}{Rr_2(\beta)}\left(\frac{1}{T}-\frac{1}{T_m}\right)\right\}\right]^{-1}. \tag{17}$$

Here $r_2(\beta)$ is a width parameter which arises from any spread in relaxation times for the dissipation process. The width of a peak measured as a function of temperature at constant frequency is determined essentially by the value of the activation energy and the value of $r_2(\beta)$. A fit of Eq. (17), including an estimate of the baseline, is shown in Fig. 5 with $E_a/r_2(\beta)=7$ kJ.mol^{-1}, $Q_m^{-1}=0.017$, and $T_m=72$ K. The value of Q_m^{-1} obtained is consistent with the observed variations in G for a relaxational process, as shown by the curve in Fig. 5 through data for the relaxed shear modulus at temperatures above 80 K. The polynomial fit and its extrapolation to low temperatures give $\Delta/2=0.016$ at 10 K using the observed value of G for C_U and the extrapolated value for C_R. If the dissipation process involves a single relaxation time, the value of β is 0 and the value of $r_2(\beta)$ is 1. In this case Eq. (14) gives $\tau_o \approx 10^{-11}$ s since the resonance peak used to determine Q^{-1} was at $f(=\tau^{-1}) \approx 830$ kHz. If there is a Gaussian spread of relaxation times, as specified by the value of β, the value of E_a will be larger and the value of τ_o smaller. For example, Figs. 4–7 of Nowick and Berry[99] gives $r_2(\beta)=1.25$ for $\beta=1$, so $E_a \approx 8.8$ kJ mol^{-1} and $\tau_o \approx 5 \times 10^{-13}$ s are obtained.

A repeat data collection on PCMO1 was designed to investigate possible hysteresis associated with the structural phase transition. Figure 6 contains peak frequency and Q^{-1} variations obtained during cooling and heating in a longer run which involved cooling from 288 to ~10 K followed by heating back to 282 K. Thermal equilibration for 15 min was allowed before data collection at each temperature and heating or cooling between set points required only a few minutes. Small differences in peak frequencies between ~200 and ~280 K are probably close to the experimental limit of resolution and may or may not be real, but the minimum in frequency occurs within 1 K of 232 K during cooling and heating, i.e., 5 K below the transition temperature determined from neutron-diffraction data.[32] The detailed data for Q^{-1} show a clear peak below the transition point with its maximum at ~215 K [Fig. 6(b)]. This peak perhaps has a sharper maximum during cooling than during heating but there is no shift in its position.

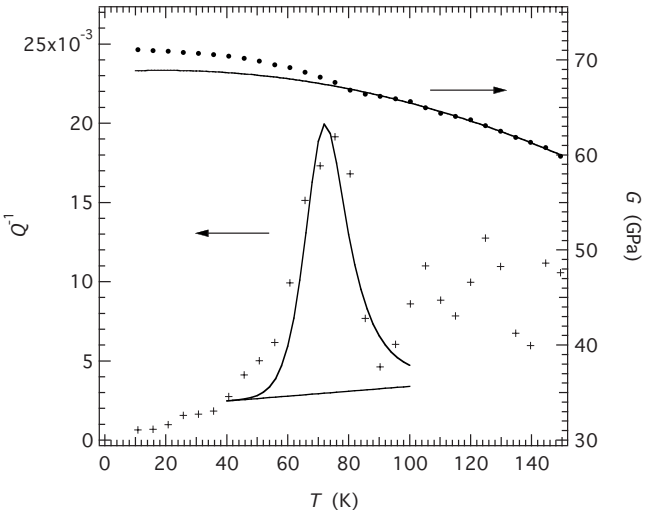

FIG. 5. Fit of Eq. (17) to data for Q^{-1} in the temperature interval 40–100 K. A linear baseline has been estimated and the fit is for $E_a/r_2(\beta)=7$ kJ mol^{-1}, $T_m=72$ K, and $Q_m^{-1}=0.017$. The curve through the data for G is the fit of a polynomial function extrapolated to $T<T_m$ and illustrates the extent of stiffening due to the Debye relaxation. It gives $\Delta/2=0.016$ at 10 K [Eqs. (15) and (16)].

RUS spectra were collected also at ~50 K intervals between room temperature and ~1130 K using sample PCMO2. There were no significant differences in the frequencies of resonance peaks during heating and cooling, so quantitative data are given here only for the cooling sequence. Frequencies of a peak near 400 kHz were determined by inspection and used to calculate the variation in G by calibration of the data as (frequency)^2 for $G=43.9$ GPa at room temperature (as above). These data are combined with data for G at low temperatures from PCMO1 in Fig. 7. They show that elastic softening ahead of the transition starts at ~1000 K. Just to show that the data can be represented by an expression of the form of Eq. (2), a curve has been fit to the data between 234 and 1021 K with G and G^o replacing $(C_{11}-C_{12})$ and $(C_{11}^o-C_{12}^o)$: $G^o=56.2\pm0.3$ GPa, $T_c=28\pm14$ K, $T_c^*=85\pm10$ K. Note, however, that $(C_{11}-C_{12})$ should tend to zero as $T\rightarrow T_c^*$ while G should tend to some constant value determined by C_{44} which is not expected to soften.

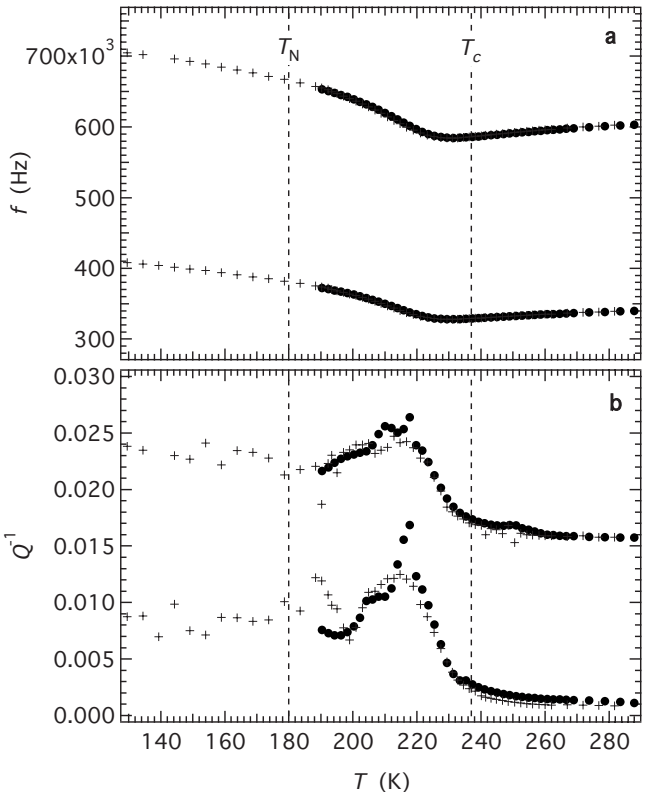

FIG. 6. Details of the variation in resonance frequency, f, and Q^{-1} for two peaks in spectra collected during cooling (filled circles) and subsequent heating (crosses) through the transition temperature (sample PCMO1). Within experimental uncertainty, there is no hysteresis in the vicinity of T_c, consistent with the transition being thermodynamically continuous. Data for Q^{-1} of the higher frequency peak have been displaced up the y axis for clarity.

C. Low temperatures, with magnetic field (Los Alamos)

Spectra were generally collected in the frequency range 300–1000 kHz with 26 000 data points per spectrum (sample PCMO2). Two different types of experiment were undertaken: varying temperature (9–283 K) at constant field and varying field (0–15 T) at constant temperature. Values of the shear modulus were extracted by calibrating the resonance frequencies of selected peaks at low frequencies using G =43.9 GPa at 293 K, as described above. This produced variations with temperature at zero field which were indistinguishable from the results obtained on the Cambridge low-temperature instrument, though with a higher degree of scatter. Results for the temperature dependence of G at constant field (0, 5, 10, and 15 T) are shown in Fig. 8(a) and at constant temperature (177, 199, 212, 225, 230, 239, 249, and 273 K) in Fig. 9(a). Corresponding variations in Q^{-1} from the same peaks as used to determine G are shown in Figs. 8(b) and 9(b). Note that, to save time, data collected at 199, 212, 239, 249, and 273 K were for a narrow frequency range (~350–500 kHz) encompassing only the first one or two resonance peaks.

The form of elastic softening and stiffening as a function of temperature at 5 and 10 T is the same as 0 T, though the minimum in G is shifted to lower temperatures with increasing field [Figs. 4 and 8(a)]. The evolution of G at 15 T is quite different, however, as the distinct minimum is no longer present. At 0, 5, and 10 T, the minimum in G is accompanied by an increase in Q^{-1} with falling temperature which is clearly identified with the structural phase transi-

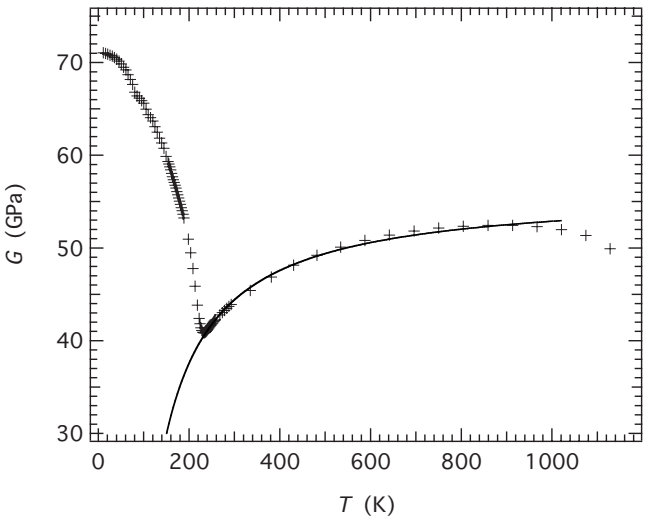

FIG. 7. Combined high-temperature (sample PCMO2) and low-temperature data (sample PCMO1) for the shear modulus, G. The curve is a fit of an expression with the form of Eq. (2) to data between 234 and 1021 K and is consistent with pseudoproper ferroelastic softening of $(C_{11}-C_{12})$ in the stability field of the *Pnma* structure.

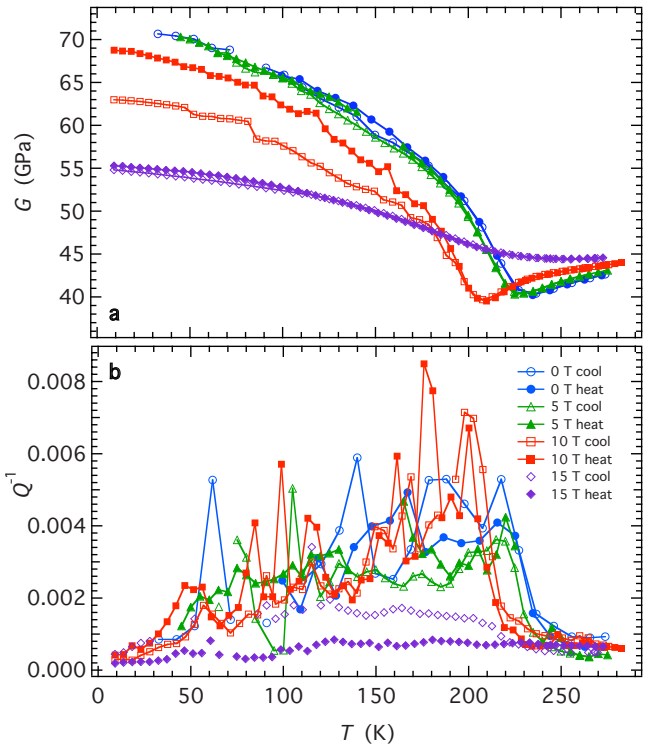

FIG. 8. (Color online) Variation in G and Q^{-1} as a function of temperature at 0, 5, 10, and 15 T (sample PCMO2). Abrupt changes in values of G for data collected at 10 T are artifacts and serve to illustrate the limit of experimental resolution.

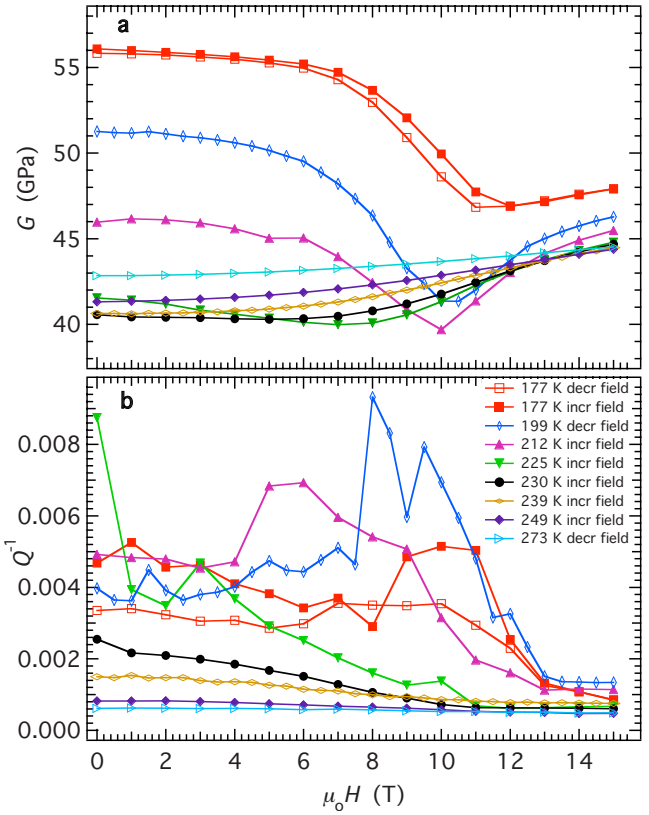

FIG. 9. (Color online) Variation in G and Q^{-1} as a function of magnetic field strength at different fixed temperatures (sample PCMO2).

tion. This peak in Q^{-1} is absent from the 15 T data and the implication is therefore that the phase transition itself is suppressed. Data for a different resonance peak in the 15 T spectra also show low Q^{-1} values at all temperatures. The pattern of variations in G at 177, 199, 212, 225, and 230 K with variable field shows the minimum in G, though this shifts to lower field and becomes less pronounced with increasing temperature [Fig. 9(a)]. The pattern of Q^{-1} is also similar for these temperatures [Fig. 9(b)], consistent with the properties of the transition being rather similar whether it is induced by varying temperature or magnetic field. At 239, 249, and 273 K, i.e., in the stability field of the *Pnma* structure, G increases slightly in a nonlinear fashion with increasing temperature [Fig. 9(a)] and Q^{-1} remains low at all field strengths [Fig. 9(b)].

From the Cambridge low-temperature data, the minimum in G occurs at ~5 K below the *Pnma*↔IC transition point. The field at which this minimum is reached when varying field strength at constant temperature, $H_{G\,min}$, and the temperature at which it is reached when varying temperature at constant field, $T_{G\,min}$, have been estimated from the data shown in Figs. 8(a) and 9(a) and are shown superimposed on a phase diagram for Pr50 from Doerr *et al.*[26] (Fig. 10). They follow the trend of the structural phase transition recognized from changes in magnetic properties of Pr50. There is hysteresis in the data, but $H_{G\,min}$ and $T_{G\,min}$ remain the same whichever way the transition is approached. A curve through the data for $H_{G\,min}$ and $T_{G\,min}$ is of the form $T_{G\,min} \propto H^4$.

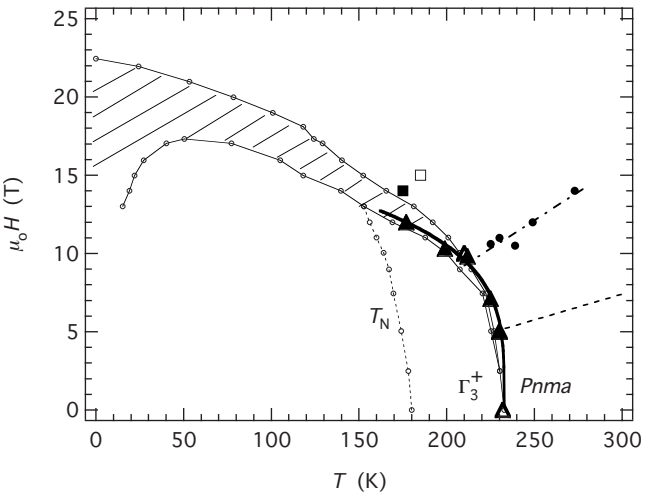

FIG. 10. Phase diagram for temperature and magnetic field strength of polycrystalline Pr50, after Doerr *et al.* (Ref. 26). The hatched area represents hysteresis limits for the insulator/ferromagnetic metal transition and the dashed line is for the metal/insulator transition in the stability field of the *Pnma* phase. Filled triangles represent the magnetic field and temperature of the minimum value of G obtained in the present study while changing temperature at fixed field for Pr48. Open triangles represent the magnetic field and temperature of the minimum value of G obtained while changing temperature at fixed field strength. The thick curved line has the form $H^4 \propto T$ through the triangles. Filled circles and the dashed-dotted line drawn through them represent the temperature and field at which $|\partial G/\partial H|$ at constant temperature reaches a maximum from the present experiments on Pr48. The open square represents the temperature at which $|\partial G/\partial T|$ has a maximum value at 15 T for Pr48 from this study, and the filled square represents the metal/insulator transition in Pr50 reported by Zheng *et al.* (Ref. 41).

At 0 and 5 T, the sample is slightly stiffer during heating than during cooling through the temperature interval ~100–180 K [Figs. 4 and 8(a)]. Similarly, at 177 K, values of G are higher during increasing field (toward the transition point) than with reducing field (away from the transition point) [Fig. 9(a)]. Data collected at 10 T were obtained by first cooling the sample in zero field and then applying a 10 T field; subsequent heating and cooling produced a much larger hysteresis than first cooling and then heating at constant field [Fig. 8(a)]. Within experimental uncertainty there is no hysteresis in the resonance frequencies obtained at 15 T, though there is perhaps a tendency for higher Q^{-1} with falling temperature than with increasing temperature at this field strength. Detailed comparison of data collected at the same temperatures and field strength during heating/cooling or during increasing/decreasing field confirmed that values of G obtained in the vicinity of the structural phase transition appear to be reproducible and fully reversible.

None of the RUS data show evidence for any influence of the antiferromagnetic phase transition on the elastic or anelastic properties of Pr48. The Néel temperature of Pr50 is near 180 K at zero field and decreases with increasing field[26] (Fig. 10). The phase diagram of Doerr *et al.*[26] (Fig. 10) has the metal/insulator transition occurring at 5–8 T in the *Pnma* stability field but there are no readily identifiable features in

the elasticity data for Pr48 corresponding with the trend line shown. Zheng *et al.*[41] have put the metal/insulator transition at ~175 K in a 14 T field, but there is again no obvious feature in the 177 K or 15 T data generated in the present study (Figs. 8 and 9), apart from a maximum in $|\partial G/\partial T|$ at ~185 K in a 15 T field.

The RUS data do not have sufficient resolution to test how the Debye peak in Q^{-1} at ~75 K responds to an external magnetic field.

V. DISCUSSION

A. Variations in elastic constants with temperature and magnetic field strength

The pattern of elastic softening for the shear modulus, G, as a function of temperature through the IC↔*Pnma* transition reported here (Fig. 4 and 7) is the same as has been found for velocities of longitudinal waves [which depend on both G and K: vel$=\sqrt{(K+\frac{4}{3}G)/\rho}$] in other polycrystalline samples of Pr50-Pr12.5 (Refs. 41 and 42) and is attributable to the softening of $(C_{11}-C_{12})$. Pseudoproper (nonlinear) softening ahead of the transition temperature is followed by a steeper nonlinear recovery below the transition point. Although a quantitative model has not been attempted, this pattern is consistent with the macroscopic perspective provided by Landau theory in Sec. II above. Bilinear coupling of the Γ_3^+ Jahn-Teller order parameter with the tetragonal strain, e_{tx}, is responsible for the pseudoproper character, and failure of G to reach lower values is understood in terms of the intervention of the symmetry-breaking incommensurate order parameter. Exactly the same pattern has been found in the evolution of G whether the transition is approached as a function of temperature in magnetic fields of progressively higher strength [Fig. 8(a)] or as a function of magnetic field strength at constant temperature [Fig. 9(a)]. From independent observations of strain evolution, the transition in Pr48 is known to be thermodynamically continuous as a function of temperature, and probably close to tricritical in character.[32] Since elastic anomalies accompanying phase transitions are highly sensitive to the mechanism and thermodynamic behavior (see, for example, Ref. 38), the clear implication is that closely similar continuous character applies when the transition point is crossed at magnetic field strengths up to at least ~12 T. This corresponds to the pattern of continuous variations in M and q_{tx} shown in Fig. 2.

In the H-T phase diagram of Pr50, the structural phase transition at $\mu_o H > \sim 2$ T involves a two-phase field and is first order in character (Fig. 10). It is marked by strong hysteresis and large changes in magnetostriction,[26] electrical resistivity,[19,20] and magnetization[20,21] at high field strengths and for temperatures at least up to 200–210 K. Seiro *et al.*[30] showed the two-phase field as appearing at 7.5 T and Saint Paul *et al.*[28] showed it as appearing at 9 T. The same pattern of large changes and hysteresis has been observed in longitudinal sound wave velocities at 160 and 52 K (Ref. 30) or below 30 K.[28] At 220 K the velocity anomaly shows a steep minimum similar in form to that shown in Fig. 7, however, as though the transition is continuous at 220 K but discontinuous at 160 K when the magnetic field is increased at constant temperature. Pr48 and Pr50 differ in that Pr50 is incommensurate below ~240 K but becomes commensurate at ~215 K (neutron diffraction from single crystal[64]) or ~170 K (electron diffraction from thin crystals[61–63]) while Pr48 remains incommensurate down to at least ~10 K (electron diffraction[53]). The neutron-diffraction result for the lock-in temperature in a bulk sample of Pr50 seems to separate the temperature intervals for continuous and discontinuous transition behavior while the wider interval of stability of the incommensurate phase in Pr48 appears to correlate with the wider temperature interval of continuous behavior. The *Pnma*↔IC transition point is slightly above the temperature or applied field value at which the shear modulus is at a minimum, but the latter gives a remarkably simple relationship between transition temperature and field strength, namely $T_{G\,min} \propto H^4$ (Fig. 10). This has the appearance of some mean-field result, though it has not yet been reconciled with an explicit behavior for $\chi(T)$ and the magnitude of the unfavorable coupling coefficient $\lambda_{qtx,M}$.

Suppression of the pseudoproper acoustic softening above the transition point with increasing magnetic field strength [Figs. 8(a) and 9(a)] is consistent with the proposed coupling between the magnetic order parameter and the Γ_3^+ order parameter set out in Sec. II above.

B. Dissipation

Significant attenuation of 8–15 MHz sound waves has previously been observed in the vicinity of the structural phase transition in Pr50 (Refs. 29 and 40) but was not followed systematically down to low temperatures. The complete pattern of variation shown by Q^{-1} at ~0.5 MHz in Figs. 4 and 6(b) is typical of the pattern of attenuation/dissipation which accompanies ferroelastic transitions and which is usually explained in terms of anelastic motion of transformation twin walls under the influence of an externally applied cyclical stress. An increase in dissipation occurs below the transition point when the twin walls become established. There then follows a plateau of relatively high dissipation due to twin wall motion constrained by an effective viscosity, which might be due to interaction with phonons.[102–105] At lower temperatures a Debye peak signifies (frequency-dependent) freezing of the twin wall motion, due to some thermally activated process such as pinning by defects. Below the freezing interval the dissipation diminishes back to a low level comparable with that of the high-temperature phase above the transition point. This behavior is well illustrated by the low-frequency anelastic response of twin walls below improper ferroelastic transitions in $(Ca,Sr)TiO_3$ and $LaAlO_3$.[105–108] Analogous behavior is seen also at RUS frequencies in $(Ca,Sr)TiO_3$,[109] $LaAlO_3$,[89] $Sr(Zr,TiO_3)$,[94,110] and $BaCeO_3$.[111]

Ferroelastic twinning due to octahedral tilting must be present in Pr48 but low dissipation above the *Pnma*↔IC transition is consistent with the observation of generally low twin wall mobility in other perovskites with *Pnma* symmetry.[94,107,109] Although the *Pnma*↔IC transition is coelastic and does not give rise to ferroelastic twinning in the same way, bilinear strain/order-parameter coupling due to the

Jahn-Teller component of the transition will give to antiphase boundaries of the IC phase some of the characteristics of a ferroelastic twin wall. In particular, the magnitude of the incommensurate repeat correlates with average Mn-O1 bond length which, in turn, correlates with the magnitude of q_{tx}.[32] This means that a shear stress which induces a strain e_{tx} will induce a change in q_{tx} and, hence, a change in the IC repeat distance, consistent with the dependence of repeat distance in $La_{0.5}Ca_{0.5}MnO_3$ thin films on strain arising from coupling with their substrate.[11] The observed dissipation can therefore be understood in terms of local displacements of the IC antiphase boundaries on a time scale of $\sim 10^{-6}$ s and is expected to be specific to $(C_{11}-C_{12})$.

If the loss mechanism relates to displacements of antiphase domain walls, the Debye peak in Q^{-1} at 72 K signifies freezing of this process due to some thermally activated step with an activation energy in the vicinity of ~ 10 kJ mol^{-1} and a characteristic relaxation time of $10^{-11}-10^{-13}$ s. Although these values are not tightly constrained, they overlap with other thermally activated processes reported in Pr,Ca manganites. Anane *et al.*[112] examined the rate of transformation from a metallic ferromagnetic state to the ordered insulator phase in Pr67 and obtained $\tau_o = 2.1 \times 10^{-11}$ s and $E_a = 11.5$ kJ mol^{-1} ($E_a/k_B = 1380$ K) for the rate controlling step. Similar activation energies have been obtained from electrical resistivity measurements in $Pr_{1-x}Ca_xMnO_3$ (Refs. 59, 113, and 114) and in $Nd_{0.5}Ca_{0.5}MnO_3$,[115] and also from electron paramagnetic resonance measurements on $La_{0.8}Ca_{0.2}MnO_3$.[116] The common step perhaps relates to migration of polarons, therefore, i.e., the migration of electrons between adjacent manganese ions with a drag due to Jahn-Teller relaxations of the structure. A similar Debye-type attenuation peak has been observed for 10 kHz longitudinal sound velocities at ~ 100 K in $Nd_{0.5}Ca_{0.5}MnO_3$ though it was attributed to paramagnetic ordering of Nd ions.[117]

The peak in Q^{-1} at ~ 215 K [Fig. 6(b)] appears to be equivalent to the characteristic peak in attenuation of ultrasonic acoustic waves just below the structural transition point of Ca-rich members of the $La_{1-x}Ca_xMnO_3$ solid solution (Refs. 27, 46, and 49; presumably all at ~ 10 MHz) and for $Nd_{0.5}Ca_{0.5}MnO_3$ (Ref. 117; 10 MHz). A similar peak has been seen at low frequencies in $La_{0.25}Ca_{0.75}MnO_3$ (Ref. 48; 0.1–10 Hz) and $Bi_{0.4}Ca_{0.6}MnO_3$,[118] the height of which varies with frequency but the peak temperature of which is independent of frequency. These features are consistent with the loss mechanism being related to the structural changes and development of a microstructure. On the basis of a reduction in the attenuation peak height with increasing magnetic field, Zheng *et al.*[27] suggested that "switching of the magnetic correlations from ferromagnetic to antiferromagnetic spin fluctuations" is important in $La_{0.5}Ca_{0.5}MnO_3$. The data for Pr48 [Fig. 8(b)] show no equivalent reduction in the maximum value of Q^{-1} between 0 and 10 T, suggesting that the loss is related to structural rather than magnetic aspects of the transition in the present case.

The plateau region between ~ 215 and ~ 90 K is the equivalent of the plateau region of attenuation associated with twin wall mobility in ferroelastic perovskites. Local displacements of IC antiphase boundaries due to the q_{tx}/e_{tx} coupling are kinetically unhindered above the freezing interval but are subject to some effective viscous drag. As with the ferroelastic twins, disruption of phonons is likely to be at least a contributory factor to this viscosity.

C. Hysteresis and relaxations of the IC structure

There is a characteristic hysteresis in the magnetization behavior and incommensurate repeat variations in the incommensurate phase of Pr48 (Refs. 53 and 54) which appears also in the shear modulus (this study) between ~ 100 and ~ 200 K. Cox *et al.*[54] argued that this hysteresis is a consequence of kinetic constraints on the evolution of the IC structure, and the newly identified Debye peak confirms that the low-temperature limit is determined by a freezing process. Similar differences to those seen on heating and cooling are seen also on increasing and reducing the external magnetic field at relatively high temperatures within the stability field of the IC structure [Fig. 9(a)]. The hysteresis is most extreme, however, when the magnetic field is changed at low temperatures, as evidenced by the data for 10 T in Fig. 8(a). When the field is applied at ~ 10 K, there is an immediate but small drop in the value of the shear modulus from ~ 70 to ~ 69 GPa. Heating and subsequent cooling returns the shear modulus to ~ 63 GPa. It is clear, therefore, that the IC structure contains two responses to temperature and magnetic field, one is displacive and effectively instantaneous and the second is thermally activated. The thermally activated component involves a rate limiting step with an activation energy and attempt frequency which appear to match values for migration of polarons and presumably relates to some degree of charge ordering.

Above the freezing interval, the normal expectation would be that the relaxation process involved in changes in charge order should be sufficiently rapid that equilibrium is achieved in times that are short in comparison with the normal heating and cooling rates. That this is not the case implies that local, metastable minima are achieved instead. Increasing temperature from a highly ordered state results in a small adjustment in the displacive component such that the order/disorder component does not achieve the same value as when starting from a relatively disordered state and lowering the temperature. The displacive component must couple with the magnetic field so that the same effect is seen in an applied field.

D. Correlation between property variations

Based on the variation in both the shear strain e_4 and the volume strain, and the temperature of the maximum in the excess heat capacity curve, the $Pnma \leftrightarrow$IC transition temperature in polycrystalline Pr48 is 237 ± 2 K.[32] This correlates closely with the highest temperature, 238 K, at which Sánchez *et al.*[53] identified an incommensurate repeat by electron diffraction in Pr48 [their Fig. 3(a)]. The minimum in RUS peak frequencies occurs at 232 ± 1 at zero field in the separate data sets from Cambridge and Los Alamos presented in this study, possibly suggesting that long-range order associated with the Γ_3^+ order parameter becomes established ~ 5 K below the temperature at which the IC structure

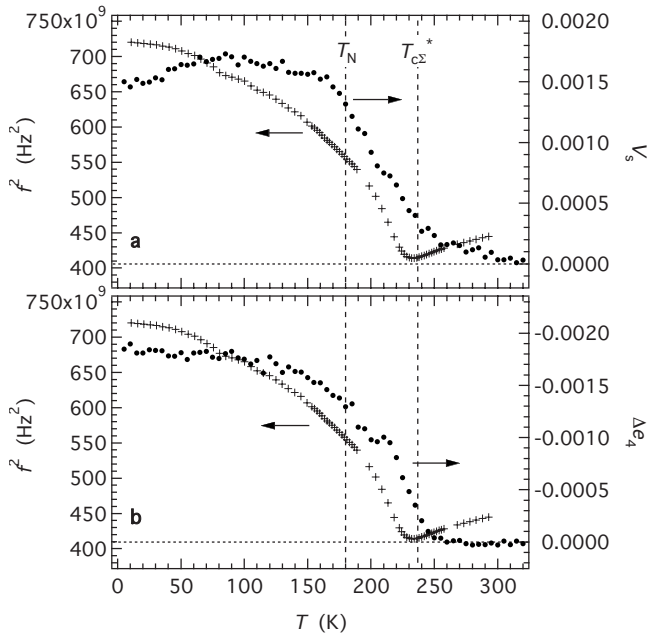

FIG. 11. Comparison of $f^2(\propto G)$ (this study) and spontaneous strains for Pr48 (from Ref. 32). The excess e_4 strain, Δe_4, does not show any obvious anomaly in the vicinity of 80 K, whereas the volume strain, V_s, shows a slight change in trend at this temperature.

becomes established. This difference is evident in Fig. 11. The transition temperature for Pr50 is ~240 K, as estimated by Kajimoto *et al.*[64] on the basis of neutron diffraction from a single crystal and by Chen *et al.*[61] on the basis of electron-diffraction observations. The minimum in longitudinal ultrasonic wave velocity through a polycrystalline sample of Pr50 occurs at ~231 K (see Fig. 4 of Ref. 41), implying that the offset is a general feature of the $Pnma \leftrightarrow$ IC transition. In the present study it has also been found that there is no hysteresis in the temperature of the minimum in G, to a precision of better than ~1 K, consistent with the transition being thermodynamically continuous.[32,54]

There are clearly premonitory effects indicated by changes in magnetization and magnetic susceptibility which start to occur at ~260 K in Pr48 (Refs. 53 and 54) and in Pr50.[56] These correlate with the onset of line broadening in powder neutron-diffraction data,[32] the onset of an excess heat capacity[54] and a tail in the volume strain [Fig. 11(b)]. The $Pnma \leftrightarrow$ IC transition thus appears to be quite normal in the sense of having short-range order or a degree of dynamic ordering in a temperature interval of ~20–30 K above the temperature at which long-range order is established and macroscopic symmetry is broken.

Line broadening in powder neutron-diffraction patterns reaches a maximum at ~210 K and diminishes to baseline values at ~170 K.[32] This maximum coincides with the maximum in the rate of change in the excess tetragonal shear strain (~220 K from differentiation of data in Ref. 32), the maximum in rate of change in the shear modulus (~215 K from differentiation of RUS frequency data) and the peak in Q^{-1}. The correlation is consistent with the view that the principal cause of elastic softening and stiffening is bilinear coupling of the tetragonal shear strain with the Γ_3^+ order parameter, q_{tx}. Line broadening is indicative of inhomogeneous development of tetragonal strain throughout the sample and Carpenter *et al.*[32] speculated that this might be due to the pre-existing twin walls from octahedral tilting transitions at higher temperatures.

There is perhaps a small anomaly in the trend of the volume strain with temperature at the expected Néel temperature but no obvious change in trend for the shear strain or shear modulus (Fig. 11, and see Fig. 8 of Ref. 32). Linear thermal-expansion data show no evidence for a change in strain at ~180 K in polycrystalline Pr50 (Ref. 26) and there is no evidence in the magnetic moment data of García-Muñoz *et al.*[21] that the antiferromagnetic transition is smeared out. It follows that any elastic relaxation accompanying the magnetic ordering is restricted to a very small volume strain. From this it follows, further, that there is likely to be little if any coupling between q_{tx} and the antiferromagnetic order parameter. Weak coupling with the volume strain should lead to a small anomaly in the bulk modulus but this may be at the level of experimental noise, even in the single-crystal elastic constant data of Hazama *et al.*[40] for Pr50. The absence of any strong coupling between the structural and antiferromagnetic order parameters also explains the lack of correlation between structural transition temperatures and magnetic transition temperatures in accumulated experimental data for the $Pr_{1-x}Ca_xMnO_3$ solid solution (Fig. 12).

The Debye peak in Q^{-1} and the related change in G at ~75 K correlate with a change in trend of the volume strain, but there is no obvious anomaly in the shear strain (Fig. 11). In polycrystalline Pr50 the same change in trend of linear strain in zero field has been seen by Doerr *et al.*[26] and there is also a shift in the longitudinal ultrasonic velocities to lower values.[41] The present data and those of Zheng *et al.*[41] are compatible if the shear modulus increases below ~80 K but the bulk modulus decreases. There do not appear to anomalies in any other physical properties at this temperature in published data for Pr48 or Pr50 so that the freezing process seems to be accompanied only by a small volume reduction. Below the freezing interval there are other anomalies, however. For example, a change in magnetization is induced by weak fields below 50 K in both Pr48 (Refs. 53 and 54) and Pr50.[113,124,126] The ac magnetic susceptibility of Pr50 displays a cusp at ~41 K which has been interpreted as a reentrant spin-glass transition that arises as a consequence of frustration between competing ferromagnetic and antiferromagnetic ordering.[124] This spin-glass transition is perhaps related to the structural freezing process, since the relaxation time at 40 K for E_a=7 kJ mol^{-1}, $\tau_o=10^{-11}$ s is 10^{-2} s [Eq. (14)], and Cao *et al.*[124] detected the magnetic anomaly using ac frequencies of $\sim 10^2-10^3$ Hz.

Close correlation between properties for polycrystalline samples is not matched by comparable correlations for properties of single crystals. In particular, the single-crystal elastic constants for Pr50 (Refs. 39 and 40) differ substantially from the bulk properties obtained here for Pr48 and by Zheng *et al.*[41] for Pr50. Apart from the large discrepancy in absolute values at room temperature discussed above, the single-crystal data for $(C_{11}-C_{12})$ have a large and apparently discontinuous change at the transition temperature together

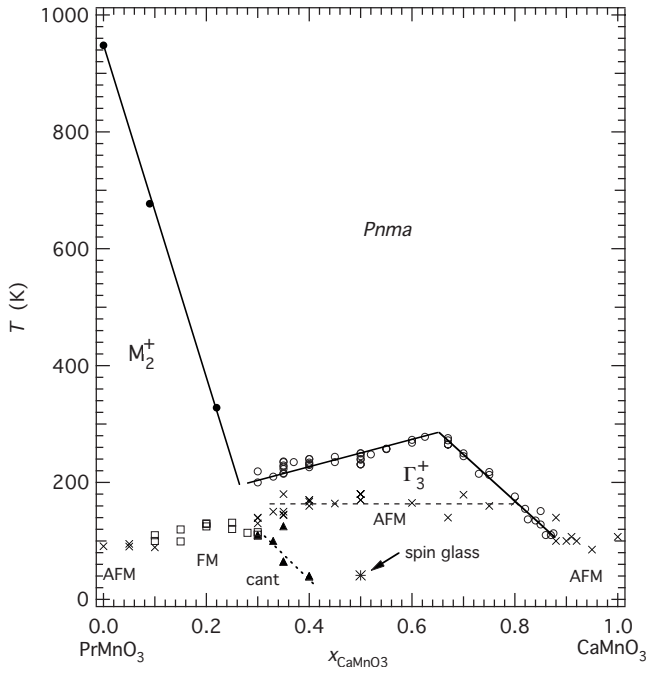

FIG. 12. Compilation of experimental data from the literature for transition temperatures in the $Pr_{1-x}Ca_xMnO_3$ solid solution. Filled circles and open circle indicate transitions to ordered structures in which the preferred Jahn-Teller ordering scheme has M_2^+ (an ordered arrangement of "Q_3" deformed octahedra) or Γ_3^+ (ordered arrangement of "Q_2" deformed octahedra) symmetry, respectively. Crystals with $X_{CaMnO3} \geq 0.5$ are expected to transform to an incommensurate structure (e.g., Refs. 53 and 59–65) while those with $X_{CaMnO3} < 0.5$ are expected to transform to a commensurate structure (e.g., Refs. 14, 60, 61, and 119). Crosses represent antiferromagnetic ordering temperatures; open squares represent ferromagnetic ordering temperatures, filled triangles represent a spin canting transition, and the star represents a spin-glass transition. Straight lines are guides to the eyes. Data from Refs. 19–22, 26, 40, 41, 56, 59, 61, 65, 118, and 120–125.

with a discontinuous reduction in the bulk modulus of more than 60%. Discontinuities in elastic constants arise at second order and tricritical transitions due to strain/order-parameter coupling of the form $\lambda e Q^2$, but such a large discontinuity in the bulk modulus seems unphysical in the light of the very small volume strain (<0.002) which accompanies the transition. Nor is the 80 K anomaly seen in the single-crystal data. Given the well-established importance of strain effects in these materials, it remains possible that grain size or interactions between grains in a polycrystalline sample are influential factors in these differences. For example, it is known that the structural phase transition is suppressed in Pr50 when the grain size is reduced below ~ 0.1 μm.[126,127] The sample used in the present study had grain sizes in the range $\sim 0.6–2.2$ μm, which is well above this limit, however, and would be expected to show the same pattern of strain and elastic behavior as occurs in other coarsely crystalline samples.

At high magnetic field strengths, Pr50 becomes metallic with respect to the temperature dependence of its electrical resistivity. Seiro *et al.*[30] associated the metal/insulator transition at temperatures above the structural transition in Pr50 with a maximum in the derivative of longitudinal acoustic velocity with respect to temperature. The same boundary appears in the *H-T* phase diagram of Doerr *et al.*[26] and is shown in Fig. 10. The maximum in $|\partial G/\partial H|$ at high temperatures has been added to Fig. 10, but does not obviously correlate with any property reported in the literature for Pr50. The only evidence for a metal/insulator transition which is separate from the structural transition appears to be provided by resistivity data of Zheng *et al.*[41] who showed it as occurring at 175 K in a 14 T field (see their Fig. 1). This is close to the maximum of $|\partial G/\partial T|$ in a 15 T field, which is at ~ 185 K in Fig. 8(a). More definitive evidence would be required to establish whether there really is a direct link between metal/insulator behavior and elastic relaxations other than at the structural phase transition.

VI. CONCLUSION

The intention of addressing the $Pnma \leftrightarrow$ IC phase transition in Pr48 from the perspective of elastic relaxations was to test the hypothesis that phase transitions involving "charge ordering," whether to commensurate or incommensurate structures, can also be understood simply in terms of multiple order parameters and their coupling with strain. From the results presented here and in Carpenter *et al.*[32] this appears to be a valid approach. Octahedral tilting plays a role, but the key order parameters relate to the zone center irrep Γ_3^+ and the zone boundary irrep Σ_1 or Σ_2. The evolution of shear strains and the volume strain conform to the pattern expected for a tricritical transition with order-parameter saturation, the shear modulus softens as the transition point is approached from either side with respect to temperature and magnetic field strength, the value of the Γ_3^+ order parameter correlates with the repeat distance of the IC structure and anelastic losses can be understood in terms of this coupling. The model is complementary to more specific microscopic models of the electronic effects (e.g., Refs. 40, 42, 128, and 129), in that it brings out the overriding constraints of symmetry as opposed to the physical origins for each order parameter. Dynamic properties related to microstructure identified through the acoustic dissipation then provide a link between the macroscopic behavior and a microscopic mechanism. On the basis of the activation energy and attempt frequency estimated from the Debye peak at 75 K, the $Pnma \leftrightarrow$ IC transition and its microstructure appear to depend on polaron kinetics in a way that implies some degree of charge order.

The present approach has differed from previous Landau descriptions in including the Γ_3^+ order parameter. Because of its bilinear coupling with the shear strain e_{tx}, an explicit signature of the operation of this order parameter is the pseudoproper ferroelastic softening of $(C_{11}-C_{12})$ ahead of the transition point. Its electronic origin is confirmed by the effect of magnetic field, which suppresses the softening. It also accounts for differences in structural behavior across the $Pr_{1-x}Ca_xMnO_3$ solid solution. The structure refinements of Jirak *et al.*[59] show that the Jahn-Teller ordering scheme of $PrMnO_3$ has the long Mn-O bond of MnO_6 octahedra arranged in a zig-zag pattern within the (010) plane (with re-

spect to *Pnma* setting), and corresponds to the M_2^+ order parameter of Carpenter and Howard.[80] Refinements of the structure of Pr48 show that this scheme starts to develop below ~800–900 K but is replaced by the Γ_3^+ scheme at ~240 K.[32] The phase diagram for structural phase transitions (Fig. 12) can therefore be understood in terms of a crossover from M_2^+ to Γ_3^+ as the preferred ordering scheme with increasing Ca content. In turn, the stability of the incommensurate structure (and its commensurate equivalent) can be ascribed to strong linear/quadratic coupling of the q_{tx} and q_Σ order parameters and strong coupling of q_{tx} with e_{tx}. Suppression of the IC structure by a strong magnetic field occurs by antipathetic (linear/quadratic) coupling of q_{tx} with the ferromagnetic order parameter.

Finally, there appears to be a continuous pathway for the transition from a structurally ordered insulator state to the ferromagnetic metal state as a function of magnetic field when the ordered state has an incommensurate structure. This contrasts with the strongly first order behavior which has been observed in $Pr_{1-x}Ca_xMnO_3$ with $\sim 0.3 < x < \sim 0.5$ and which provides a structural mechanism for CMR.

ACKNOWLEDGMENTS

The RUS facilities in Cambridge were established through a grant from the Natural Environment Research Council of Great Britain (Grant No. NE/B505738/1 to M.A.C.). Neil Mathur and Casey Israel are thanked for introducing M.A.C. to manganites. Work at NHMFL-PFF, Los Alamos was performed under the auspices of the National Science Foundation, the State of Florida, and U.S. Department of Energy.

[1] M. A. Carpenter, E. K. H. Salje, and A. Graeme-Barber, Eur. J. Mineral. **4**, 621 (1998).
[2] A. J. Millis, T. Darling, and A. Migliori, J. Appl. Phys. **83**, 1588 (1998).
[3] J. P. Attfield, Chem. Mater. **10**, 3239 (1998).
[4] N. D. Mathur and P. B. Littlewood, Solid State Commun. **119**, 271 (2001).
[5] R. Y. Gu and C. S. Ting, Phys. Rev. B **65**, 214426 (2002).
[6] A. R. Bishop, T. Lookman, A. Saxena, and S. R. Shenoy, Europhys. Lett. **63**, 289 (2003).
[7] M. J. Calderón, A. J. Millis, and K. H. Ahn, Phys. Rev. B **68**, 100401(R) (2003).
[8] G. C. Milward, M. J. Calderón, and P. B. Littlewood, Nature (London) **433**, 607 (2005).
[9] K. H. Ahn, T. Lookman, A. Saxena, and A. R. Bishop, Phys. Rev. B **71**, 212102 (2005).
[10] J. P. Chapman, J. P. Attfield, L. M. Rodriguez-Martinez, L. Lezama, and T. Rojo, Dalton Trans. **2004**, 3026 (2004).
[11] S. Cox, E. Rosten, J. C. Chapman, S. Kos, M. J. Calderón, D.-J. Kang, P. B. Littlewood, P. A. Midgley, and N. D. Mathur, Phys. Rev. B **73**, 132401 (2006).
[12] K. Dörr, O. Bilani-Zeneli, A. Herklotz, A. D. Rata, K. Boldyreva, J.-W. Kim, M. C. Dekker, K. Nenkov, L. Schultz, and M. Reibold, Eur. Phys. J. B **71**, 361 (2009).
[13] T. Z. Ward, J. D. Budai, Z. Gai, J. Z. Tischler, L. Yin, and J. Shen, Nat. Phys. **5**, 885 (2009).
[14] P. G. Radaelli, G. Iannone, D. E. Cox, M. Marezio, H. Y. Hwang, and S.-W. Cheong, Physica B **241-243**, 295 (1998).
[15] F. Zhong and Z. D. Wang, Phys. Rev. B **61**, 3192 (2000).
[16] Z. Q. Li, X. H. Zhang, J. S. Yu, X. J. Liu, X. D. Liu, H. Liu, P. Wu, H. L. Bai, C. Q. Sun, J. J. Lin, and E. Y. Jiang, Phys. Lett. A **325**, 430 (2004).
[17] Y. Tokura, Rep. Prog. Phys. **69**, 797 (2006).
[18] I. Kézsmárki, Y. Tomioka, S. Miyasaka, L. Demkó, Y. Okimoto, and Y. Tokura, Phys. Rev. B **77**, 075117 (2008).
[19] Y. Tomioka, A. Asamitsu, H. Kuwahara, Y. Moritomo, and Y. Tokura, Phys. Rev. B **53**, R1689 (1996).
[20] M. Tokunaga, N. Miura, Y. Tomioka, and Y. Tokura, Phys. Rev. B **57**, 5259 (1998).
[21] J. L. García-Muñoz, M. Respaud, C. Frontera, A. Llobet, J. M. Broto, H. Rakoto, and C. Goiran, J. Appl. Phys. **85**, 5570 (1999).
[22] K. S. Nagapriya, A. K. Raychaudhuri, B. Bansal, V. Venkataraman, S. Parashar, and C. N. R. Rao, Phys. Rev. B **71**, 024426 (2005).
[23] J. M. De Teresa, M. R. Ibarra, C. Marquina, P. A. Algarabel, and S. Oseroff, Phys. Rev. B **54**, R12689 (1996).
[24] Yu. F. Popov, A. M. Kadomtseva, G. O. Vorob'ev, K. I. Kamilov, V. Yu. Ivanov, A. A. Mukhin, and A. M. Balbashov, Phys. Solid State **43**, 1533 (2001).
[25] G. Reményi, M. Doerr, M. Loewenhaupt, S. Sahling, M. Saint-Paul, and P. Lejay, Physica B **346-347**, 83 (2004).
[26] M. Doerr, G. Reményi, M. Rotter, S. Sahling, M. Saint-Paul, and M. Loewenhaupt, J. Magn. Magn. Mater. **290-291**, 906 (2005).
[27] R. K. Zheng, C. F. Zhu, and X. G. Li, Phys. Status Solidi A **184**, 251 (2001).
[28] M. Saint-Paul, G. Reményi, P. Lejay, P. Monceau, G. Chouteau, and S. de Brion, J. Magn. Magn. Mater. **272-276**, 2096 (2004).
[29] S. Seiro, H. R. Salva, M. Saint-Paul, A. A. Ghilarducci, P. Lejay, P. Monceau, M. Nunez-Regueiro, and A. Sulpice, J. Phys.: Condens. Matter **14**, 3973 (2002).
[30] S. Seiro, G. Reményi, M. Saint-Paul, H. R. Salva, A. A. Ghilarducci, P. Monceau, and P. Léjay, Mater. Sci. Eng., A **370**, 384 (2004).
[31] H. Fujishiro, M. Ikebe, T. Kikuchi, and T. Fukase, Physica B **378-380**, 518 (2006).
[32] M. A. Carpenter, R. E. A. McKnight, C. J. Howard, and K. S. Knight, Phys. Rev. B **82**, 094101 (2010).
[33] C. J. Howard and M. A. Carpenter, Acta Crystallogr., Sect. B: Struct. Sci. **66**, 40 (2010).
[34] W. Rehwald, Adv. Phys. **22**, 721 (1973).
[35] B. Lüthi and W. Rehwald, in *Structural Phase Transitions*, edited by K. A. Muller and H. Thomas, Topics in Current Physics (Springer-Verlag, Berlin, 1981), Vol. 23, p. 131.
[36] P. A. Fleury and K. Lyons, in *Structural Phase Transitions*, edited by K. A. Muller and H. Thomas, Topics in Current Physics (Springer-Verlag, Berlin, 1981), Vol. 23, p. 9.
[37] E. K. H. Salje, *Phase Transitions in Ferroelastic and Coelastic*

Crystals (Cambridge University Press, Cambridge, 1993).
[38] M. A. Carpenter and E. K. H. Salje, Eur. J. Mineral. **10**, 693 (1998).
[39] H. Hazama, Y. Nemoto, T. Goto, Y. Tomioka, A. Asamitsu, and Y. Tokura, Physica B **312-313**, 757 (2002).
[40] H. Hazama, T. Goto, Y. Nemoto, Y. Tomioka, A. Asamitsu, and Y. Tokura, Phys. Rev. B **69**, 064406 (2004).
[41] R. K. Zheng, G. Li, Y. Yang, A. N. Tang, W. Wang, T. Qian, and X. G. Li, Phys. Rev. B **70**, 014408 (2004).
[42] C. X. Chen, T. Qian, R. K. Zheng, F. Wang, and X. G. Li, Phys. Status Solidi B **241**, 1827 (2004).
[43] A. P. Ramirez, P. Schiffer, S.-W. Cheong, C. H. Chen, W. Bao, T. T. M. Palstra, P. L. Gammel, D. J. Bishop, and B. Zegarski, Phys. Rev. Lett. **76**, 3188 (1996).
[44] A. P. Ramirez, S.-W. Cheong, and P. Schiffer, J. Appl. Phys. **81**, 5337 (1997).
[45] C. Zhu, R. Zheng, J. Su, and W. Shong, J. Phys.: Condens. Matter **12**, 823 (2000).
[46] R. K. Zheng, C. F. Zhu, J. Q. Xie, and X. G. Li, Phys. Rev. B **63**, 024427 (2000).
[47] R. K. Zheng, R. X. Huang, A. N. Tang, G. Li, X. G. Li, J. N. Wei, J. P. Shui, and Z. Yao, Appl. Phys. Lett. **81**, 3834 (2002).
[48] R. K. Zheng, A. N. Tang, Y. Yang, W. Wang, G. Li, X. G. Li, and H. C. Ku, J. Appl. Phys. **94**, 514 (2003).
[49] X. G. Li, R. K. Zheng, G. Li, H. D. Zhou, R. X. Huang, J. Q. Xie, and Z. D. Wang, Europhys. Lett. **60**, 670 (2002).
[50] C. X. Chen, R. K. Zheng, T. Qian, Y. Liu, and X. G. Li, J. Phys. D: Appl. Phys. **38**, 807 (2005).
[51] C. X. Chen, G. S. Jiang, J. L. Jiang, Q. L. Zhang, and R. K. Zheng, J. Magn. Magn. Mater. **308**, 71 (2007).
[52] C. X. Chen, J. Y. Zheng, Y. Y. Jiang, J. Li, and R. K. Zheng, Physica B **405**, 2088 (2010).
[53] D. Sánchez, M. J. Calderón, J. Sánchez-Benítez, A. J. Williams, J. P. Attfield, P. A. Midgley, and N. D. Mathur, Phys. Rev. B **77**, 092411 (2008).
[54] S. Cox, J. C. Lashley, E. Rosten, J. Singleton, A. J. Williams, and P. B. Littlewood, J. Phys. Condens. Matter **19**, 192201 (2007).
[55] S. Cox, J. C. Loudon, A. J. Williams, J. P. Attfield, J. Singleton, P. A. Midgley, and N. D. Mathur, Phys. Rev. B **78**, 035129 (2008).
[56] S. Krupicka, M. Marysko, Z. Jirák, and J. Hejtmánek, J. Magn. Magn. Mater. **206**, 45 (1999).
[57] H. T. Stokes, D. M. Hatch, and B. J. Campbell, ISOTROPY, 2007, http://stokes.byu.edu/isotropy.html
[58] H. T. Stokes, D. M. Hatch, and H. M. Nelson, Phys. Rev. B **47**, 9080 (1993).
[59] Z. Jirák, S. Krupicka, Z. Simsa, M. Dlouhá, and S. Vratislav, J. Magn. Magn. Mater. **53**, 153 (1985).
[60] M. v. Zimmermann, C. S. Nelson, J. P. Hill, D. Gibbs, M. Blume, D. Casa, B. Keimer, Y. Murakami, C.-C. Kao, C. Venkataraman, T. Gog, Y. Tomioka, and Y. Tokura, Phys. Rev. B **64**, 195133 (2001).
[61] C. H. Chen, S. Mori, and S.-W. Cheong, Phys. Rev. Lett. **83**, 4792 (1999).
[62] S. Mori, T. Katsufuji, N. Yamamoto, C. H. Chen, and S.-W. Cheong, Phys. Rev. B **59**, 13573 (1999).
[63] Z. Jirák, F. Damay, M. Hervieu, C. Martin, B. Raveau, G. André, and F. Bourée, Phys. Rev. B **61**, 1181 (2000).
[64] R. Kajimoto, H. Yoshizawa, Y. Tomioka, and Y. Tokura, Phys. Rev. B **63**, 212407 (2001).
[65] Z. Jirák, C. Martin, M. Hervieu, and J. Hejtmánek, Appl. Phys. A: Mater. Sci. Process. **74**, s1755 (2002).
[66] R. Feile, A. Loidl, and K. Knorr, Phys. Rev. B **26**, 6875 (1982).
[67] K. Knorr, A. Loidl, and J. K. Kjems, Physica B **136**, 311 (1986).
[68] H. Hazama, T. Goto, Y. Nemoto, Y. Tomioka, A. Asamitsu, and Y. Tokura, Phys. Rev. B **62**, 15012 (2000).
[69] P. Norby, I. G. Krogh Andersen, E. Krogh Andersen, and N. H. Andersen, J. Solid State Chem. **119**, 191 (1995).
[70] J. Rodríguez-Carvajal, M. Hennion, F. Moussa, A. H. Moudden, L. Pinsard, and A. Revcolevschi, Phys. Rev. B **57**, R3189 (1998).
[71] P. Mandal, B. Bandyopadhyay, and B. Ghosh, Phys. Rev. B **64**, 180405 (2001).
[72] P. Mandal and B. Ghosh, Phys. Rev. B **68**, 014422 (2003).
[73] M. C. Sánchez, G. Subías, J. García, and J. Blasco, Phys. Rev. Lett. **90**, 045503 (2003).
[74] T. Chatterji, F. Fauth, B. Ouladdiaf, P. Mandal, and B. Ghosh, Phys. Rev. B **68**, 052406 (2003).
[75] T. Chatterji, B. Ouladdiaf, P. Mandal, and B. Ghosh, Solid State Commun. **131**, 75 (2004).
[76] T. Chatterji, D. Riley, F. Fauth, P. Mandal, and B. Ghosh, Phys. Rev. B **73**, 094444 (2006).
[77] X. Qiu, Th. Proffen, J. F. Mitchell, and S. J. L. Billinge, Phys. Rev. Lett. **94**, 177203 (2005).
[78] M. A. Carpenter and C. J. Howard, Acta Crystallogr., Sect. B: Struct. Sci. **65**, 147 (2009).
[79] M. A. Carpenter, C. J. Howard, B. J. Kennedy, and K. S. Knight, Phys. Rev. B **72**, 024118 (2005).
[80] M. A. Carpenter and C. J. Howard, Acta Crystallogr. B **65**, 134 (2009).
[81] A. Daoud-Aladine, J. Rodríguez-Carvajal, L. Pinsard-Gaudart, M. T. Fernández-Díaz, and A. Revcolevschi, Appl. Phys. A: Mater. Sci. Process. **74**, s1758 (2002).
[82] A. Daoud-Aladine, J. Rodríguez-Carvajal, L. Pinsard-Gaudart, M. T. Fernández-Díaz, and A. Revcolevschi, Phys. Rev. Lett. **89**, 097205 (2002).
[83] L. Wu, R. F. Klie, Y. Zhu, and Ch. Jooss, Phys. Rev. B **76**, 174210 (2007).
[84] Ch. Jooss, L. Wu, T. Beetz, R. F. Klie, M. Beleggia, M. A. Schofield, S. Schramm, J. Hoffmann, and Y. Zhu, Proc. Natl. Acad. Sci. U.S.A. **104**, 13597 (2007).
[85] E. Salje, Phys. Chem. Miner. **12**, 93 (1985).
[86] E. Salje, B. Kuscholke, B. Wruck, and H. Kroll, Phys. Chem. Miner. **12**, 99 (1985).
[87] E. Salje and V. Devarajan, Phase Transitions **6**, 235 (1986).
[88] F. Camara, M. A. Carpenter, M. C. Domeneghetti, and V. Tazzoli, Am. Mineral. **88**, 1115 (2003).
[89] M. A. Carpenter, A. Buckley, P. A. Taylor, and T. W. Darling, J. Phys.: Condens. Matter **22**, 035405 (2010).
[90] A. S. Borovik-Romanov and H. Grimmer, *Physical properties of crystals*, International Tables for Crystallography Vol. D, edited by A. Authier (Kluwer Academic, Dordrecht, 2003).
[91] E. Fawcett and R. C. Sherwood, Phys. Rev. B **1**, 4361 (1970).
[92] R. E. A. McKnight, M. A. Carpenter, T. W. Darling, A. Buckley, and P. A. Taylor, Am. Mineral. **92**, 1665 (2007).
[93] R. E. A. McKnight, T. Moxon, A. Buckley, P. A. Taylor, T. W. Darling, and M. A. Carpenter, J. Phys.: Condens. Matter **20**, 075229 (2008).
[94] R. E. A. McKnight, C. J. Howard, and M. A. Carpenter, J. Phys.:

Condens. Matter **21**, 015901 (2009).
[95] A. Migliori and J. L. Sarrao, *Resonant Ultrasound Spectroscopy: Applications to Physics, Materials Measurements and Nondestructive Evaluation* (Wiley, New York, 1997).
[96] A. Migliori and J. D. Maynard, Rev. Sci. Instrum. **76**, 121301 (2005).
[97] H. Ledbetter, M. Lei, A. Hermann, and Z. Sheng, Physica C **225**, 397 (1994).
[98] J. J. U. Buch, G. Lalitha, T. K. Pathak, N. H. Vasoya, V. K. Lakhani, P. V. Reddy, R. Kumar, and K. B. Modi, J. Phys. D: Appl. Phys. **41**, 025406 (2008).
[99] A. S. Nowick and B. S. Berry, *Anelastic Relaxation in Crystalline Solids* (Academic, New York, 1972).
[100] M. Weller, G. Y. Li, J. X. Zhang, T. S. Kê, and J. Diehl, Acta Metall. **29**, 1047 (1981).
[101] *Mechanical Spectroscopy* Q^{-1} 2001 with Applications to Materials Science, edited by R. Schaller, G. Fantozzi, and G. Gremaud (Trans Tech, Brandain, Switzerland, 2001).
[102] J. A. Combs and S. Yip, Phys. Rev. B **28**, 6873 (1983).
[103] Y. N. Huang, Y. N. Wang, and H. M. Shen, Phys. Rev. B **46**, 3290 (1992).
[104] Y. N. Wang, Y. N. Huang, H. M. Shen, and Z. F. Zhang, J. Phys. IV **6**, C8-505 (1996).
[105] R. J. Harrison, S. A. T. Redfern, and E. K. H. Salje, Phys. Rev. B **69**, 144101 (2004).
[106] R. J. Harrison and S. A. T. Redfern, Phys. Earth Planet. Inter. **134**, 253 (2002).
[107] R. J. Harrison, S. A. T. Redfern, and J. Street, Am. Mineral. **88**, 574 (2003).
[108] R. J. Harrison, S. A. T. Redfern, A. Buckley, and E. K. H. Salje, J. Appl. Phys. **95**, 1706 (2004).
[109] J. N. Walsh, P. A. Taylor, A. Buckley, T. W. Darling, J. Schreuer, and M. A. Carpenter, Phys. Earth Planet. Inter. **167**, 110 (2008).
[110] R. E. A. McKnight, B. J. Kennedy, Q. Zhou, and M. A. Carpenter, J. Phys.: Condens. Matter **21**, 015902 (2009).
[111] Z. Zhang, J. Koppensteiner, W. Schranz, J. B. Betts, A. Migliori, and M. A. Carpenter, Phys. Rev. B **82**, 014113 (2010).
[112] A. Anane, J.-P. Renard, L. Reversat, C. Dupas, P. Veillet, M. Viret, L. Pinsard, and A. Revcolevschi, Phys. Rev. B **59**, 77 (1999).
[113] M. R. Lees, J. Barratt, G. Balakrishnan, D. McK. Paul, and C. D. Dewhurst, J. Phys.: Condens. Matter **8**, 2967 (1996).
[114] L. M. Fisher, A. V. Kalinov, I. F. Voloshin, N. A. Babushkina, K. I. Kugel, and D. I. Khomskii, J. Magn. Magn. Mater. **258-259**, 306 (2003).
[115] T. Vogt, A. K. Cheetham, R. Mahendiran, A. K. Raychaudhuri, R. Mahesh, and C. N. R. Rao, Phys. Rev. B **54**, 15303 (1996).
[116] A. Shengelaya, G.-M. Zhao, H. Keller, K. A. Müller, and B. I. Kochelaev, Phys. Rev. B **61**, 5888 (2000).
[117] L. Jiang, J. Su, H. Kong, Y. Liu, S. Zheng, and C. Zhu, J. Phys.: Condens. Matter **18**, 8563 (2006).
[118] W. J. Lu, Y. P. Sun, B. C. Zhao, X. B. Zhu, and W. H. Song, Phys. Rev. B **73**, 214409 (2006).
[119] H. Yoshizawa, H. Kawano, Y. Tomioka, and Y. Tokura, J. Phys. Soc. Jpn. **65**, 1043 (1996).
[120] O. Yanagisawa, M. Izumi, W.-Z. Hu, K. Nakanishi, and H. Nojima, J. Supercond. **12**, 307 (1999).
[121] M. R. Lees, O. A. Petrenko, G. Balakrishnan, and D. McK. Paul, Phys. Rev. B **59**, 1298 (1999).
[122] C. Martin, A. Maignan, M. Hervieu, and B. Raveau, Phys. Rev. B **60**, 12191 (1999).
[123] T. Tonogai, T. Satoh, K. Miyano, Y. Tomioka, and Y. Tokura, Phys. Rev. B **62**, 13903 (2000).
[124] G. Cao, J. Zhang, S. Wang, J. Yu, C. Jing, S. Cao, and X. Shen, J. Magn. Magn. Mater. **301**, 147 (2006).
[125] A. M. L. Lopes, J. P. Araújo, V. S. Amaral, J. G. Correia, Y. Tomioka, and Y. Tokura, Phys. Rev. Lett. **100**, 155702 (2008).
[126] T. Zhang and M. Dressel, Phys. Rev. B **80**, 014435 (2009).
[127] Z. Jirák, E. Hadová, O. Kaman, K. Knížek, M. Marysko, E. Pollert, M. Dlouha, and S. Vratislav, Phys. Rev. B **81**, 024403 (2010).
[128] R. L. Melcher, Phys. Acoust. **12**, 1 (1976).
[129] G. C. Rout and S. Panda, J. Phys.: Condens. Matter **21**, 416001 (2009).